AD-A128 927 MEASUREMENTS OF DIRECT PATH AND FOLDED PATH OPTICAL SCINTILLATION PATH WEIGHTINGS(U) NAVAL POSTGRADUATE SCHOOL MONTEREY CA A G COSTANTINE JUN 83 1/1

UNCLASSIFIED F/G 20/6 NL

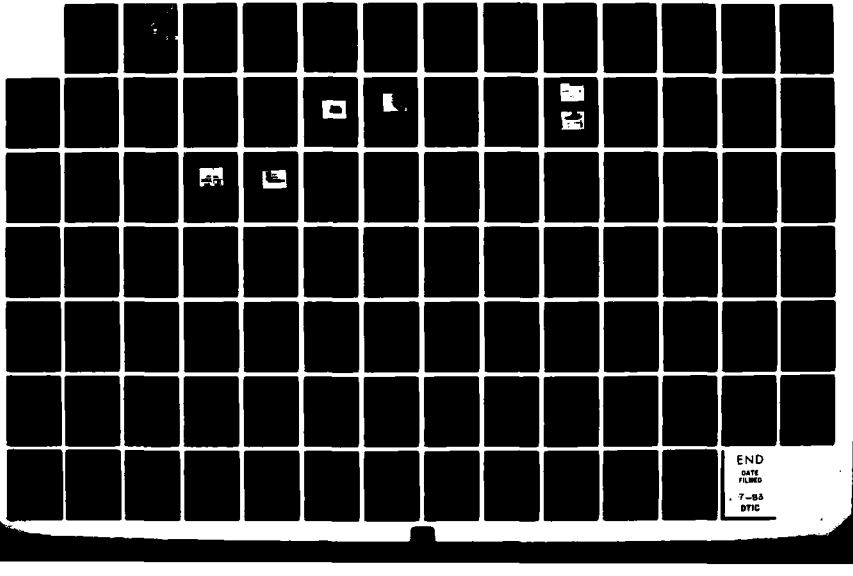

END
DATE FILMED
7-83
DTIC

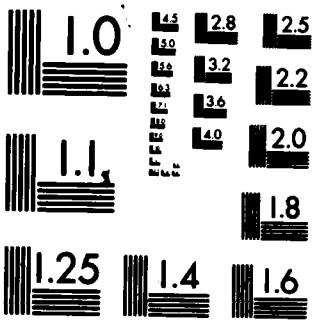

NAVAL POSTGRADUATE SCHOOL
Monterey, California

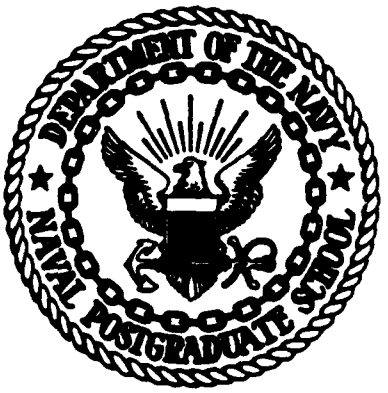

THESIS

MEASUREMENTS OF DIRECT PATH AND FOLDED PATH OPTICAL SCINTILLATION PATH WEIGHTINGS

by

Alfred Guy Costantine

June 1983

Thesis Advisor: E. A. Milne

Approved for public release; distribution unlimited

Unclassified
SECURITY CLASSIFICATION OF THIS PAGE (When Data Entered)

REPORT DOCUMENTATION PAGE		READ INSTRUCTIONS BEFORE COMPLETING FORM
1. REPORT NUMBER	2. GOVT ACCESSION NO. A128927	3. RECIPIENT'S CATALOG NUMBER
4. TITLE (and Subtitle) Measurements of Direct Path and Folded Path Optical Scintillation Weightings		5. TYPE OF REPORT & PERIOD COVERED Master's Thesis June 1983
		6. PERFORMING ORG. REPORT NUMBER
7. AUTHOR(s) Alfred G. Costantine		8. CONTRACT OR GRANT NUMBER(s)
9. PERFORMING ORGANIZATION NAME AND ADDRESS Naval Postgraduate School Monterey, California 93940		10. PROGRAM ELEMENT, PROJECT, TASK AREA & WORK UNIT NUMBERS
11. CONTROLLING OFFICE NAME AND ADDRESS Naval Postgraduate School Monterey, California 93940		12. REPORT DATE June 1983
		13. NUMBER OF PAGES 93
14. MONITORING AGENCY NAME & ADDRESS(if different from Controlling Office)		15. SECURITY CLASS. (of this report) Unclassified
		15a. DECLASSIFICATION/DOWNGRADING SCHEDULE

16. DISTRIBUTION STATEMENT (of this Report)

Approved for public release; distribution unlimited

17. DISTRIBUTION STATEMENT (of the abstract entered in Block 20, if different from Report)

18. SUPPLEMENTARY NOTES

19. KEY WORDS (Continue on reverse side if necessary and identify by block number)

Scintillation Path Weighting

20. ABSTRACT (Continue on reverse side if necessary and identify by block number)

A theoretical prediction by Dr. Avihu Ze'evi of the relative contribution to the optical scintillation by different points along the path was described by a weight function for direct and exact folded path spherical wave sources. In an effort to verify this prediction a turbulence chamber was built to allow a controlled turbulence source to be moved and measured at different path positions in conjunction with scintillation

(continued)

DD FORM 1 JAN 73 1473 EDITION OF 1 NOV 65 IS OBSOLETE
S/N 0102-LF-014-6601

Unclassified
SECURITY CLASSIFICATION OF THIS PAGE (When Data Entered)

Item 20. (continued)

measurements. The experimental results follow Dr. Ze'evi's general pattern but both sources are less weighted at the detector end than predicted and the folded path is more heavily weighted at the target end than predicted.

Approved for public release; distribution unlimited

Measurements of Direct Path and Folded Path Optical Scintillation Path Weightings

by

Alfred Guy Costantine
Captain, United States Army
B.S., United States Military Academy, 1973

Submitted in partial fulfillment of the
requirements for the degree of

MASTER OF SCIENCE IN PHYSICS

from the

NAVAL POSTGRADUATE SCHOOL
June 1983

Author: Alfred G Costantine

Approved by: Edmund A Milne
Thesis Advisor

P. A. Sturtevant Jr.
Second Reader

G R Schacher
Chairman, Department of Physics

John Dyer
Dean of Science and Engineering

ABSTRACT

A theoretical prediction by Dr. Avihu Ze'evi of the relative contribution to the optical scintillation by different points along the path was described by a weight function for direct and exact folded path spherical wave sources. In an effort to verify this prediction a turbulence chamber was built to allow a controlled turbulence source to be moved and measured at different path positions in conjunction with scintillation measurements. The experimental results follow Dr. Ze'evi's general pattern but both sources are less weighted at the detector end than predicted and the folded path is more heavily weighted at the target end than predicted.

TABLE OF CONTENTS

ACKNOWLEDGEMENTS

The author would like to express his sincere appreciation to a variety of sources without whose help the completion of this project would not have been possible. The timely and precise work of Robert C. Moeller, Model Maker, in building and repairing system components was commendable. The assistance of Robert J. Flenniken, and the advice of Michael C. Drong in the experimental phase were invaluable. The guidance of Professor E. C. Crittenden insured our analysis was thorough and complete.

Finally, a special note of thanks is given to Professor E. A. Milne who freely gave of his time to instruct the author in scintillation experimental procedures, constantly provided sage guidance, and inspired the author through his obvious zeal for scientific research.

I. INTRODUCTION

A. BACKGROUND

In optical propagation through the atmosphere the varying fluctuations of refractive index cause random deviations in phase across a propagation wavefront. This change of the refractive index is observed as the "twinkling" of stars or the "image boil" of lasers and is known as scintillation. Scintillation results from the random ray bending with its associated interference manifesting desultory irradiance fluctuations at an observation plane.

Theoretically, in the weak turbulence region an accepted model of scintillation for spherical waves is the normalized log amplitude variance [Ref. 1] given by:

$$\sigma_\kappa^2 = 0.125\ K^{7/6}\ C_n^2\ \ L^{11/6}$$

where

$K = 2\pi/\lambda$, λ is the optical wavelength

L = Path length from source to detector

C_n^2 = Refractive index structure constant (a direct measure of the level of atmospheric turbulence)

Experimentally, scintillation can be measured by placing a point detector in the observation plane and registering irradiance level fluctuations with time. Scintillation strength can be calculated by the variance of the normalized intensity (irradiance), as follows:

$$\sigma^2_{I/I_o} = \langle (I/I_o)^2 \rangle - \langle I/I_o \rangle^2$$

$$= [\langle I^2 \rangle - \langle I \rangle^2]/I_o^2$$

$$= \sigma_I^2/I_o^2$$

where

$I = I(r,t)$ is the instantaneous intensity on the receiver

$\sigma_I^2 = \langle I^2 \rangle - \langle I \rangle^2$

$I_o = \langle I(r, t) \rangle$ is the ensemble average

Tatarski [Ref. 1] found that in regions of weak turbulence the log irradiance fluctuation was also Gaussian distributed. Thus we use experimental measurements of the log intensity variance to determine the scintillation as below:

$$\ell = \log (I/I_o)$$

$$\sigma_\ell^2 = \langle l^2 \rangle - \langle l \rangle^2$$

$$\sigma_\ell^2 = \langle (\log I/I_o)^2 \rangle - \langle \log I/I_o \rangle^2$$

$$= \langle (\log I - \log I_o)^2 \rangle - \langle \log I - \log I_o \rangle^2$$

$$= \langle (\log I - \log I_o)\ (\log I - \log I_o) \rangle -$$

$$\langle \log I - \log I_o \rangle \langle \log I - \log I_o \rangle$$

$$= \langle (\log I)^2 - 2 \log (I_o + I) + (\log I_o)^2 \rangle -$$

$$[(\langle \log I \rangle)^2 - \langle 2 \log I_o \log I \rangle + (\langle \log I_o \rangle)^2]$$

$$= \langle (\log I)^2 \rangle - 2 \log I_o \langle \log I \rangle + (\log I_o)^2 - \langle \log I \rangle^2$$

$$+ 2 \log I_o \langle \log I \rangle - (\log I_o)^2$$

$$= \langle (\log I)^2 \rangle - \langle \log I \rangle^2$$

$$\sigma_\ell^2 = \sigma^2_{\text{Log } I}$$

This allows the scintillation to be described by the variance of log intensity fluctuations received at a detector with no dependence on the average signal intensity received.

Clifford notes [Ref. 2] that the relationship $\sigma_\ell^2 = 4\sigma_\kappa^2$ is the accepted formula to correlate the empirical (σ_ℓ^2) and the theoretical (σ_κ^2) variances. This results in our being able to describe the scintillation for spherical waves in the low turbulence region by:

$$\sigma_\ell^2 = 0.52\ K^{7/6}\ C_n^2\ \ L^{11/6}$$

where $\sigma^2 \lesssim 1$ defines the low turbulence region.

B. PATH WEIGHTING THEORY

The works of Tatarski [Ref. 1], Fried [Ref. 3], Clifford [Ref. 2, 4],Lutomirski and Yura [Ref. 5], Fante [Ref. 6] and others have led to a fairly clear understanding of the processes involved for scintillation on a direct path. Experimental results are reasonably close to theoretical predictions for direct path scintillation. The problem of scintillation on folded paths is less understood, and theoretical predictions of existing theories have not been fully confirmed by experimental evidence.

In his doctoral dissertation at the Naval Postgraduate School, Dr. Avihu Ze'evi investigated the special case of optical scintillation on folded paths displaced a small angle (θ) from the direct laser path. This investigation examined spherical waves and a plane mirror as a folding target. In particular, Ze'evi stated that for the direct path (one-way) laser and the exact ($\theta = 0$) folded path laser, the relative

contribution to the scintillation of different points along the path is described by the weight function. Ze'evi stated that the weight functions $W_i(x)$ for spherical waves are:

For direct path $W_L(x) = [x(1-x)]^{5/6}$

For the folded path $W_F(x) = [x(2-x)]^{5/6}$

Figure 1 shows the optics layout for the direct path and exact folded path lasers. The two path-weighting functions are shown in Figure 2.

From Figure 2 we can see that in the case of the exact folded path ($\theta = 0$), the main contribution to the scintillation comes from the vicinity of the mirror. In the case of the single path, the main contribution is from the center of the path. Ze'evi further noted that it was very unlikely that we could find the proper conditions under which $C_n^2(x)$ along an atmospheric path is constant, and that we should be careful when we compare results from two types of path.

The development and use of a controlled environment chamber to test Ze'evi's predicted scintillation path weighting functions for the direct path and exact folded path spherical waves was the main goal of this experiment.

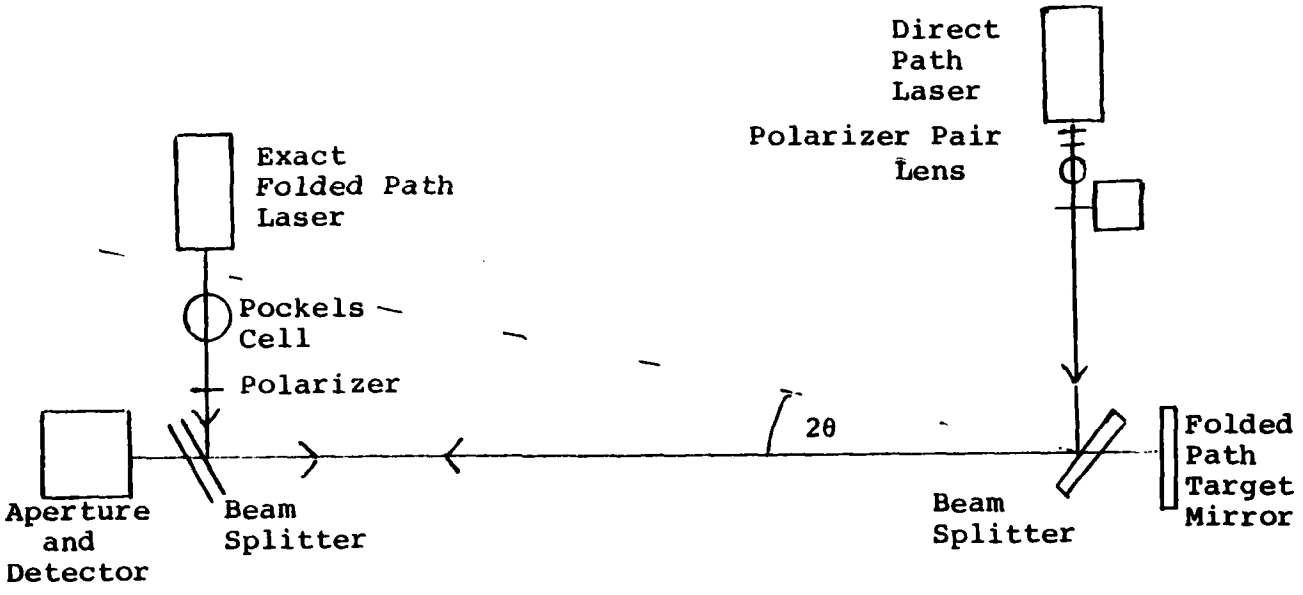

Figure 1. Optical Equipment Layout. Solid lines show layout for the exact folded path ($\theta=0$) used throughout this experiment. Dashed lines defines the angle θ for cases where $\theta \neq 0$.

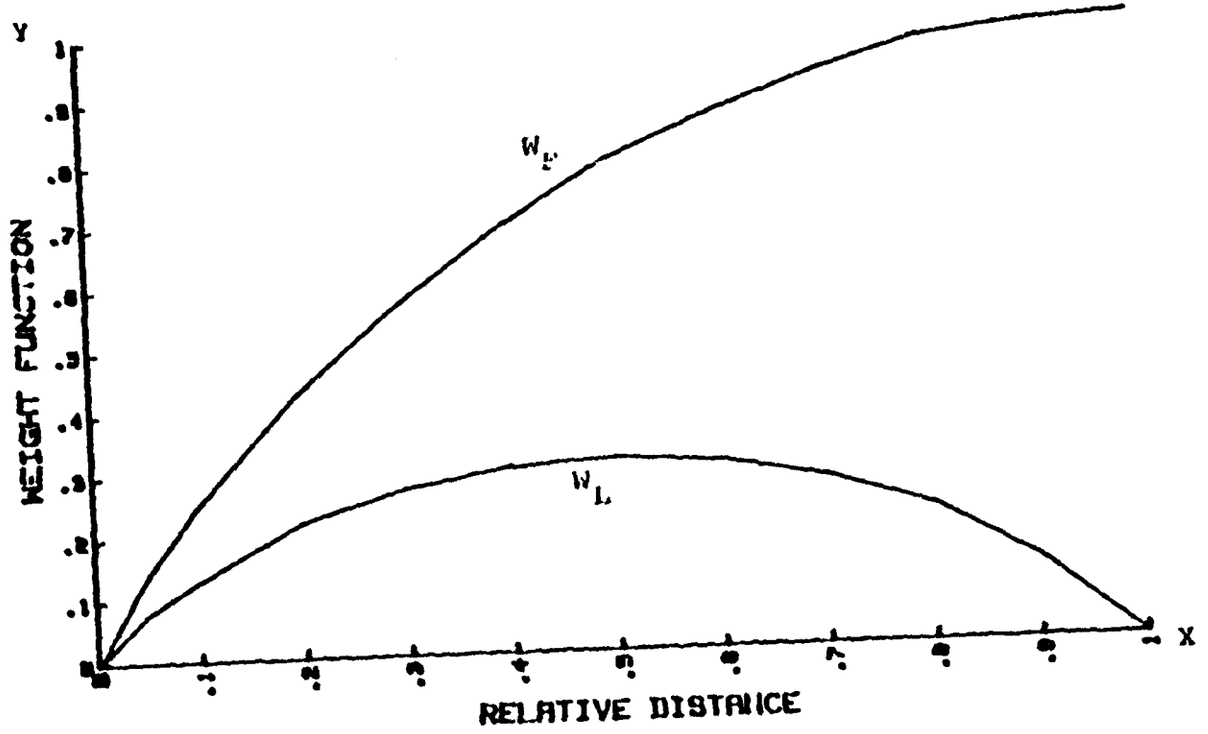

Figure 2. The Weight Functions of Spherical Waves in the Cases of a Single Path (W_L) and a Folded Path with $\theta = 0$ (W_F). x represents the relative location along the path. For single path; the source at $x = 0$ and the detector at $x = 1$. For folded path; the source and the detector are at $x = 0$, the mirror is at $x = 1$.

II. EXPERIMENTAL APPROACH

A. GENERAL CONSIDERATIONS

As a result of the continuing experimental studies at the Naval Postgraduate School into the effect of turbulent atmosphere on optical propagation [Ref. 8] and the attempts by Hodgini [Ref. 9], and Speer and Parker [Ref. 10] to validate portions of Ze'evi's doctoral dissertation we began our analysis with access to experimental apparatus designed to measure scintillation for direct path and folded path lasers. As a result of observing the efforts of Speer and Parker we realized a controlled environment was essential to produce meaningful results in an analysis of scintillation path weighting. The turbulence source used to cause scintillation along our path needed to be as uniform as possible, measurable for C_T^2 in order to normalize our results, and capable of being positioned at different locations along the laser propagation path. Additionally, the optics needed to be isolated from air currents (wind) that had caused vibrations in past experiments and thus introduced added uncertainties to the results. For these reasons we decided to add a turbulence chamber to the existing apparatus. This chamber consisted of a "tunnel", a controlled turbulence source with a method for measuring C_T^2 of the disturbance, and protection for the system's optical components. With these considerations in mind we will now begin an analysis of the entire experimental apparatus to measure the scintillation during our experiment.

B. TURBULENCE CHAMBER

The basic concept for the turbulence chamber called for eliminating turbulence and vibrations to optical components unless we caused the turbulence at a known location in the system and could measure this turbulence. The following components comprised our turbulence chamber:

1. Tunnel

A 61 meter long tunnel of .61 meter height and .61 meter width was constructed by joining 25 sections of 2.44 m by .61 m by .61 m boxes made of 1/4 inch plywood. To prepare the tunnel for possible outdoor use the plywood was treated with a water sealant and painted white on the exterior to lessen the diurnal heating effects. The tunnel interior was painted flat black to eliminate reflections. Our experiment, however, was conducted in the 145 meter basement of Spanagel Hall thus rendering some of these precautions unnecessary. To allow access to basement laboratories the individual boxes were only joined together to form a tunnel for the actual experimental runs. Box seams and the edges that mated to other boxes were sealed with 76 mm wide insulation tape to eliminate unwanted turbulence entrance. One tunnel section was modified to house the turbulence source and will be discussed later.

2. Turbulence Source

The turbulence source was chosen by Flenniken [Ref. 11] to insure we operated in an isotropic turbulence region. The turbulence source consisted of a heat element connected to a

powerstat output to control the amount of heat produced. The heat element was mounted on ceramic insulators below a screen with .0015 meter square meshing (Figure 3) to break the turbulence into small evenly distributed patterns. At a setting of 70 volts the heater produced a local air temperature of 27-30 celsius at 22 cm above the screen.

The turbulence source was mounted in a modified tunnel section (Figure 4) to insure its configuration would remain essentially constant and to ease in relocating the turbulence source during experiments. A relatively simple procedure was devised where this section could be entered into the tunnel at a desired location and the tunnel taped together thus creating a constant tunnel configuration with only the turbulence location changing. For our experiments the turbulence source was introduced at 1.0, 5.8, 10.7, 15.5, 20.4, 25.3, 30.1, 35.0, 39.8, 44.7, 49.5, 54.4, and 60.0 meters from the detector. This change of turbulence location could be completed in several minutes without disturbing or adjusting any optical components involved in the experiment. The actual configuration of the modified tunnel section evolved throughout this experiment as a result of our desire to isolate the turbulence section from the hallway environmental influences as much as possible. Modifications will be discussed in the experimental section.

3. Turbulence Measurement Equipment

It was our desire to have the turbulence we caused to be as constant as feasible. Realizing the random nature of the

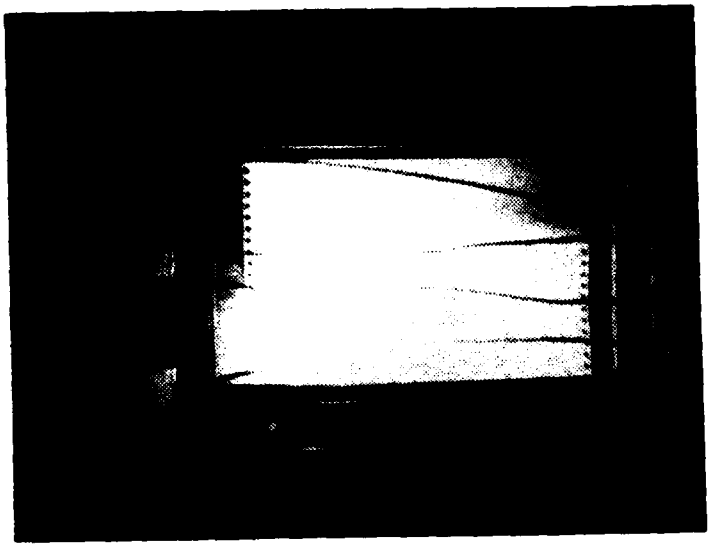

Figure 3. Heat Source Showing the Heat Element Mounted Below the Screen

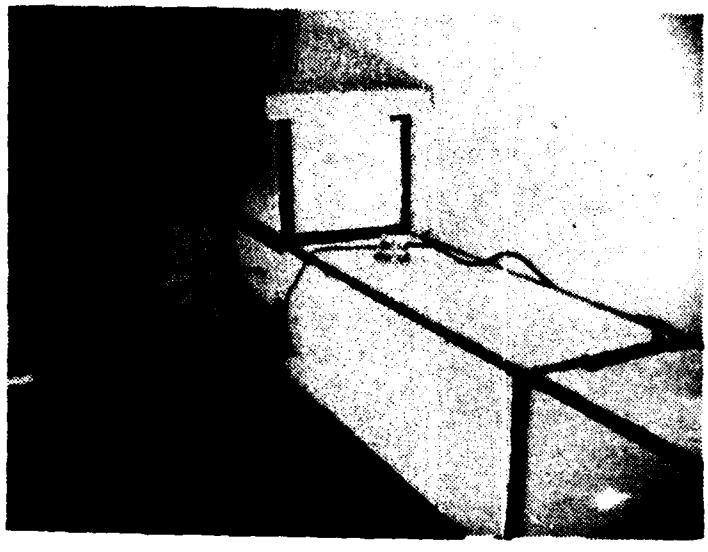

Figure 4. Optics Protection Cap Joined to the Modified Tunnel Section that Housed the Heating Source. The platinum probes for C_T^2 measurement are shown entering the tunnel just above the baffle. Heat source tunnel section has chimney and roof mounted.

heat dissipation we chose to measure the temperature structure index C_T^2 and then normalize our measured experimental variance for the fluctuations of C_T^2 at the different path locations. C_T^2 was measured by inserting 2 platinum probes spared 6 cm apart a height of 22 cm above the heat source screen. The platinum probes were sampled at a rate of 11 Hertz and 500 samples were taken to compute C_T^2 . This provided a 45 second sampling period in which to compute an accurate picture of the temperature structure index. Four such runs were made and averaged at each heat source location just prior to collecting scintillation data. Figure 5 shows the equipment utilized to process the data from the platinum probes. For details on the operation the equipment utilized to calculate C_T^2 see Reference 11.

4. Optics Protection

To attempt to eliminate unwanted turbulence from the tunnel and prevent the possibility of air currets vibrating our optics we capped the tunnel ends (Figure 6). Because of the size of our optics the end caps had to be larger than the .61m x .61m tunnel section so we chose standard laboratory tables large enough to house the optics and boxed off the legs with the same type plywood used to construct the tunnel. These were taped in an effort to stop all turbulence and light leaks. During experimental runs these end caps were taped to the tunnel and all data and power wires to the optics were run under the back entrance to the caps and tape was utilized to seal possible turbulence entrances.

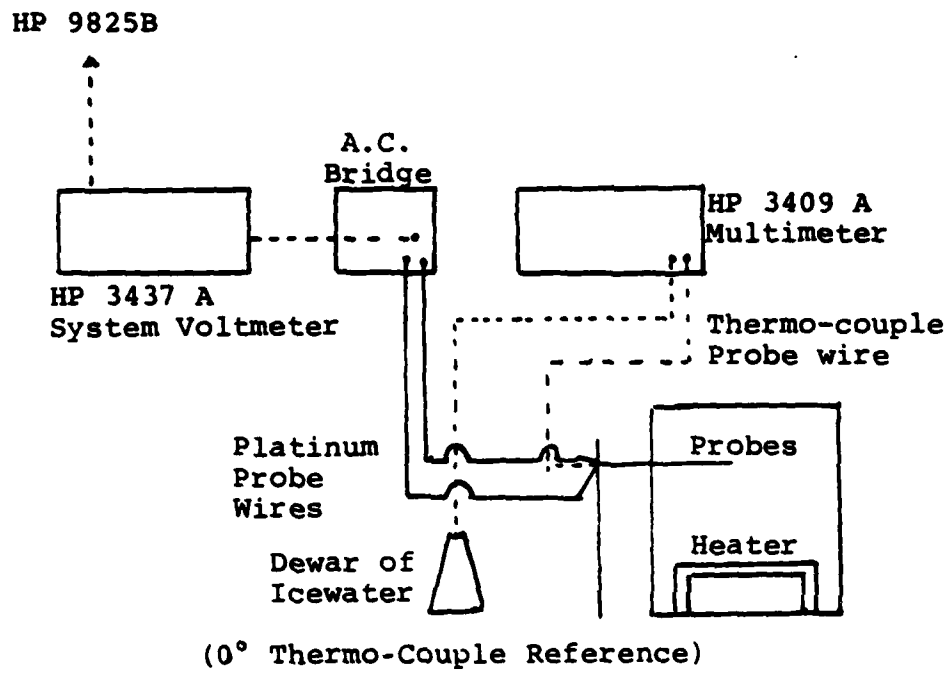

Figure 5. C_T^2 Calculation Layout

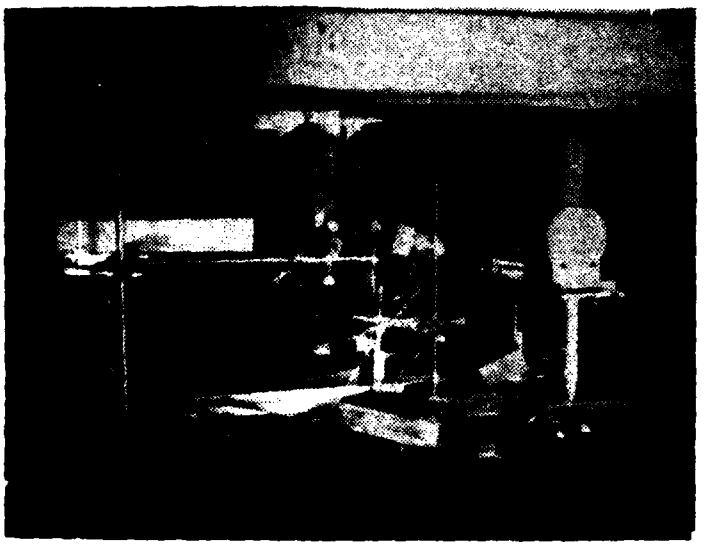

Optics Cap for Target End of Tunnel. From left, direct path laser, polarizer pair, lens, chopper direct path beam splitter, and folded path target mirror.

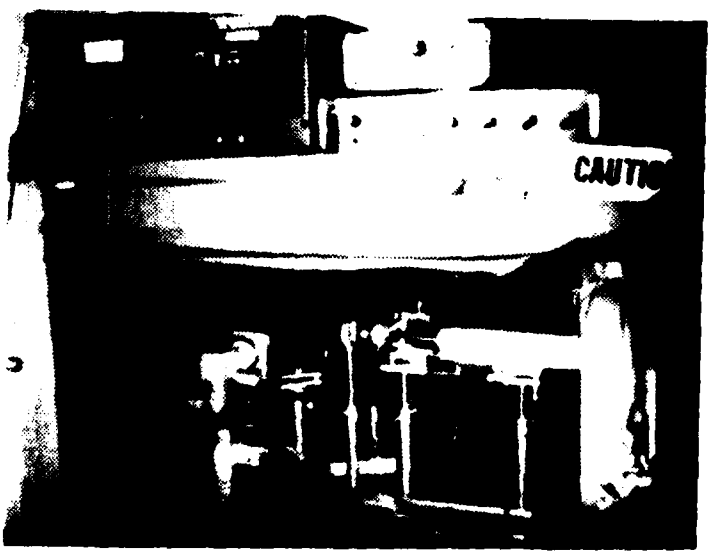

Optics Cap for Detector End of Tunnel. From left, detector, folded path beam splitter, polarizer, Pockels cell, and laser. Note Pockels modulation system, PAR, and high voltage on top of optics cap.

Figure 6. Open Optics Caps

C. OPTICAL EQUIPMENT

The optical setup utilized is illustrated in Figure 1. The target end consisted of the direct path laser, whose intensity was controlled by use of two polarizers. Next, the direct path beam was diverged by a lens, and modulatd by a mechanical chopper. The modulated beam was then reflected down the tunnel to the detector aperture by a beam splitter. Located directly behind the beam splitter was the target mirror for the folded path. The detector end optics consisted of the folded path laser, Pockels cell modulator, a polarizer, a beam splitter to cause the direct path and folded path beams to be coincident as the folded path beam travelled the tunnel, passed through the direct path splitter, reflected off the target mirror and returned down the tunnel on the same path to the detector as the direct path laser. The aperture and detector were located behind the folded path splitter.

1. Laser Sources

The two lasers used throughout the experiment were HeNe lasers with a wavelength of .6328 micrometers. The low output of these lasers, .95 milliwatt, made them eyesafe and thus reduced the safety hazard and associated problems in both alignment and operation. Both lasers were mounted on platforms controlled by micrometer screw adjustments to facilitate precision alignment. It was essential to utilize laser sources whose internal stability would be such as not to effect the scintillation we were measuring. Hodgini measured

the source variances of these lasers as less than 3×10^{-4}, and ratio of the source variance of these two lasers was .996 [Ref. 9]. Although the lasers were noted to become unstable with time, the correlation of the two sources when chopped alternately with a pulse separation of 0.3 milliseconds over the same optical path did not, and thus they could be used together in measuring scintillation with some confidence that their internal instability would not contribute to the scintillation we were measuring.

2. Target End Optics

The target end optics consisted of a set of adjustable polarizers for fine signal intensity reductions to match the direct path intensity to that of the folded path laser. A lens was utilized to expand the beam to prevent beam wander from affecting the scintillation measurements. The four-inch beam splitter was a half-inch thick optical window with an advertised flatness correct to 1/10 of a wavelength and parallelism within two seconds of arc. An antireflective coating was applied and one side of the splitter silvered to allow 50 percent transmission. The target mirror for the folded path laser was a five inch optical flat of good optical flatness.

3. Detector End Optics

The folded path beam passed immediately through a coherent Associates Model 3003 Modulation System Pockels cell. This Pockels cell in conjunction with the polarizer that the beam passed through next were used to modulate the laser beam.

D. PULSE FORMING AND DETECTION EQUIPMENT

The pulse forming equipment in our experiment included a mechanical chopper with an open to close ratio of 1:4 that rotated at a 3000 rpm rate. This provided a chopping frequency of 1000 Hertz. The chopper rotation modulated a light emitting diode mounted opposite a detector. The detector sent a trigger signal sent to a Pulse/Function Generator thus establishing the timing for the entire system. This trigger signal was then delayed for .4 milliseconds before triggering the Pockels Cell Modulation System for the folded path laser. This timing allowed the direct path and folded path lasers to arrive sequentially at the detector aperture. The aperture size was 3 millimeters and this was well within the 6.2 millimeters required to be within the first Fresnel Zone. Zone size was calculated as follows:

$$\ell_F = (\lambda L)^{1/2}$$

ℓ_F is the Fresnel zone radius

λ = .6328 micrometers

L = 61 meters

By utlizing an aperture size smaller than the Fresnel Zone and smaller than the 10.2 mm lateral coherency length for our HeNe lasers we approximated our detector as a point detector in the observation plane. For a more detailed discussion of the choice of a 3 millimeter aperture see Reference 9.

Signals passing through the aperture were focused on the detector. The detector was an RCA silicon photodiode type

C30872. When operated at 370 volts this detector provided an extremely high signal to noise ratio without the need for cooling.

Next the output of the detector was amplified by a Princeton Applied Research (PAR) Model 113 Low Noise Amplifier capable of yielding a signal gain of up to 10000. Additionally, the PAR had an adjustable bandwidth with high and low frequency roll-offs. The roll-offs were carefully set to eliminate system noise without distorting the signal sent to the processing equipment. Figure 7 gives a schematic layout of the pulse forming and detection equipment plus the respective signal channeling to the signal processing and data reduction equipment.

E. SIGNAL PROCESSING EQUIPMENT

The PAR output signal was sent directly to the direct path and folded paths demodulators. A trigger pulse activated the demodulator to demodulate only its respective input signal. The demodulator utilized a sample and hold to take the instantaneous maximum of the incoming signal. The background signal was subtracted from the instantaneous maximum and this difference was output from the demodulator. This differential output meant that the true maximum signal intensity was available for further processing. Figure 8 shows the signal forms and timing sequence of the demodulator waveforms.

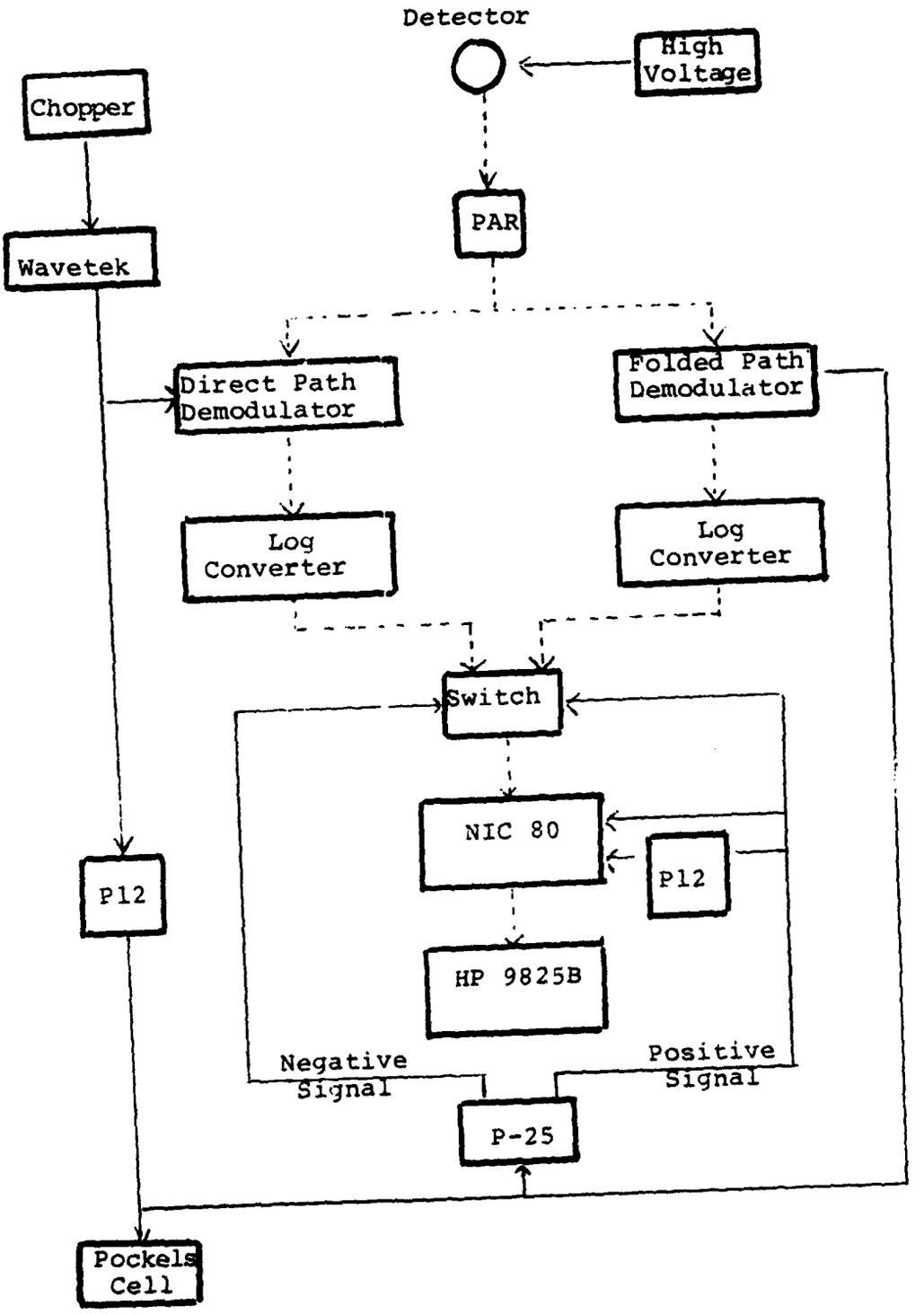

Figure 7. Diagram of Pulse Forming, Processing, and Data Reduction Equipment

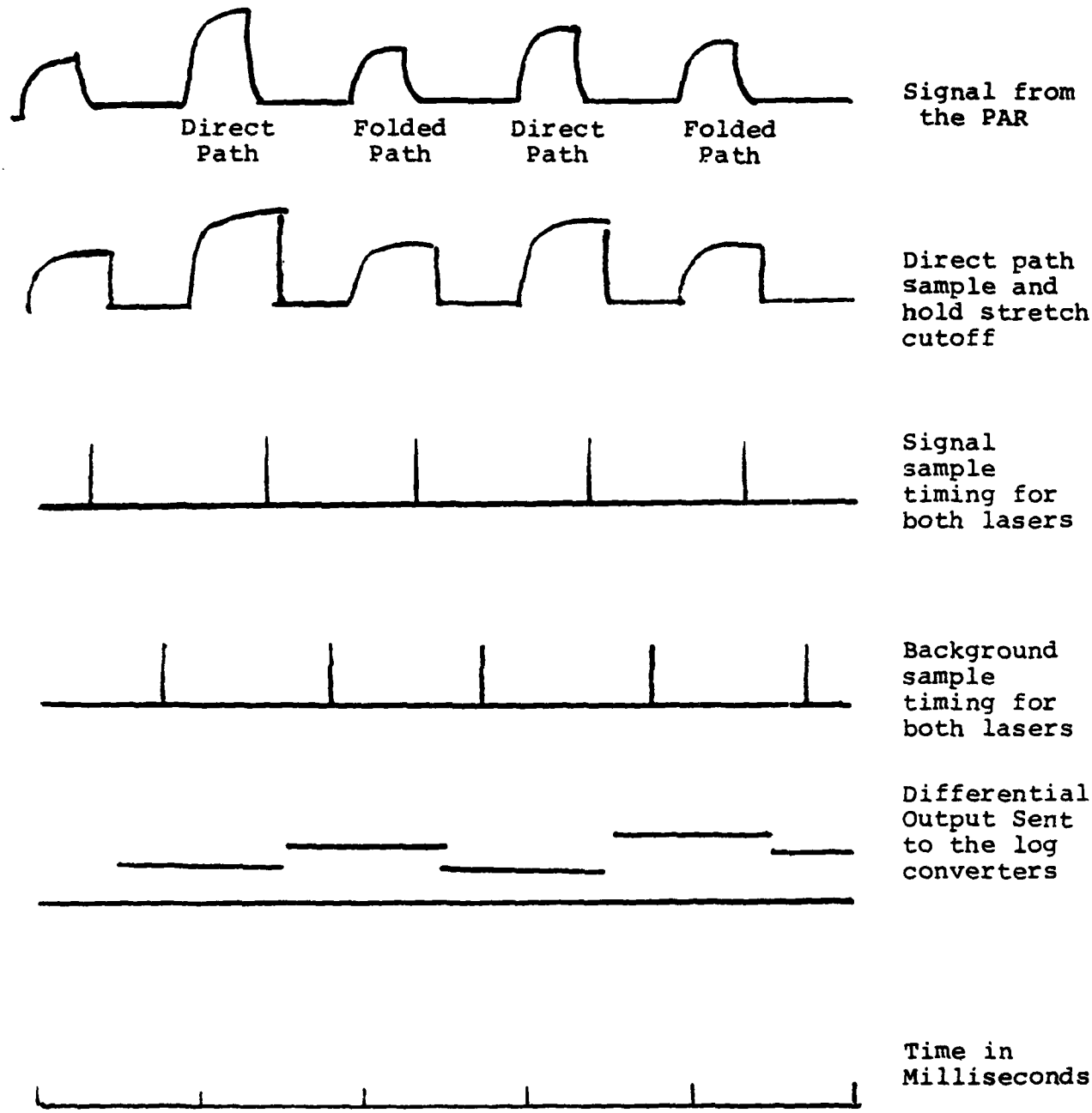

Figure 8. Shape and Timing of Demodulator Waveforms

The differential output of the demodulators was sent to the direct and folded path's respective Hewlett-Packard Model 7562A Log Converters since we desired to have the log intensity variance as the actual measure of the scintillation.

Finally, these processed signals had to be fed to the data reduction system in order to calculate the scintillation. This process was complicated by the fact that the Nicolet 1080 (NIC80) Stored Program Computer had only one analog to digital converter port. To time share this port for use by both laser signals the Atmospheric Physics Group at the Naval Postgraduate School had built an electronic switch which allowed the Nicolet 1080 to accept both the direct path and folded path signals. Details of this switch operator are available in Reference 10. Figure 9 shows the Signal Processing Equipment layout.

F. DATA REDUCTION EQUIPMENT

The computer system used to analyze the signal was composed of four components: The Nicolet Instrument Corporation Model NIC-80; the Hewlett Packard (HP) 9825B Caclulator; the HP-9871A Printer; and the HP9862A Calculator Plotter. Figure 10 shows the Data Reduction Equipment setup.

The program for the NIC-80 is available in Reference 10. During experimental runs the NIC-80 built a histogram of the number of counts versus point signal intensity for each laser. This was accomplished for four separate runs at each heater location. Each run consisted of 16,384 samples per laser

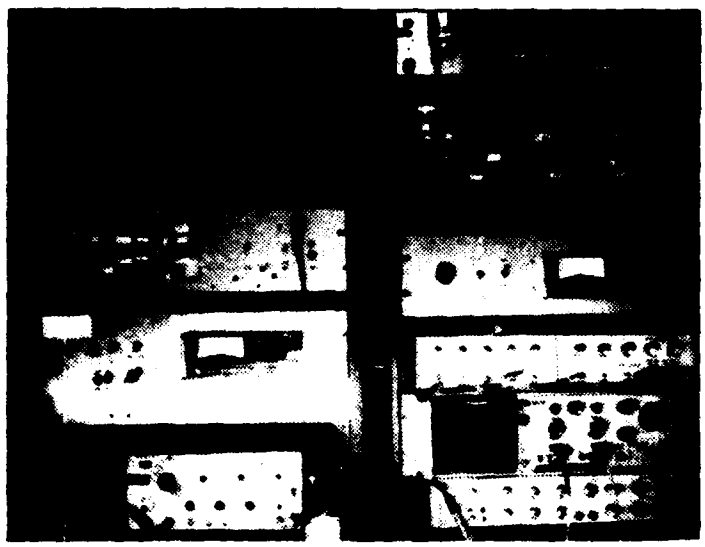

Figure 9. Signal Processing Equipment

Left bay, top to bottom: Direct path demodulator, direct path log converter, and wavetek signal generator.

Right bay, top to bottom: Electronic switch, folded path demodulator, folded path log converter, P-12's, oscilliscope, and P-25.

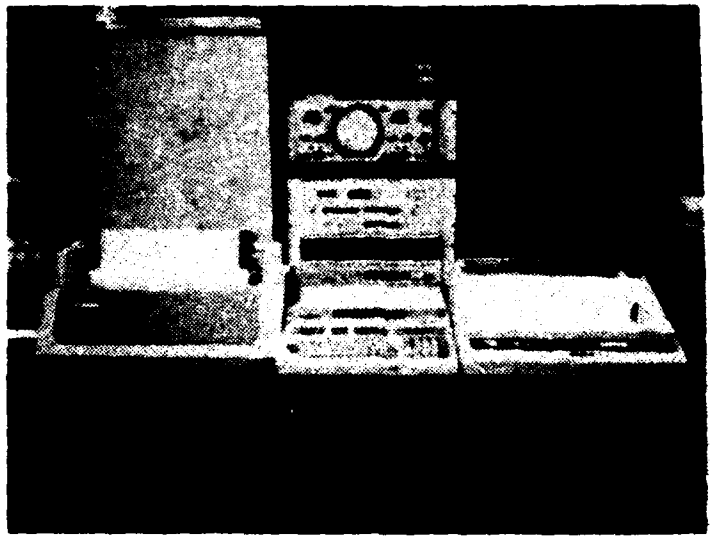

Figure 10. Data Reduction Equipment

Front row from left: HP 9871A printer, HP 9825B calculator, and HP 9862A calculator plotter. Background, Nicolet 1080.

source. At the end of the four runs this data was transferred to magnetic tapes loaded in the HP-9825B for storage and statistical analysis upon operator command.

The HP-9825B calculator was the system controller for the NIC-80, the printer, and the plotter. Control of the NIC-80 was achieved through a computer interface designed by Professor Edmund Milne at NPS. The HP9825-B scintillation program is presented in Reference 10.

To calculate the statistical parameters we desired the intensity distributions from each run were loaded from their magnetic tape storage locations and the HP-9825B processed them in accordance with accepted formulas for mean, variance, standard deviation, and chi-square. Speer [Ref. 10] determined the for a 95% confidence interval the chi-square calculation with a goodness of fit parameter of 288.87 or less was necessary to assume our log normal curve corresponded to a true Gaussian curve.

Upon completion of the statistics calculation the HP9825B automatically caused the printer to list header information detailing the date the experiment was conducted, the fact that the aperture was in place (AP), the detector avalanche voltage, PAR bandpass, and the fact the tests were for the exact folded path (0). All runs were conducted with a PAR gain of 500. Additionally, the time the runs began were noted as well as the turbulence source distance from the detector. In the columns below this are listed the number of data points that actually

comprise the historgram, the variance, and the chi-square value. Four runs were conducted at each location and in each case the direct path laser parameters are listed first, then the folded path parameters.

Upon completion of the statistics printout of each run, the HP9825B presented the operator a choice of an immediate plot of the data or a continuation of the statistics calculations. The plotter graphically displayed the actual point by point histogram that the NIC-80 had built then drew a solid line to show a true normal curve calculated by the chi-square approach. Samples of the statistical printouts for these experiments are presented in Appendix A through D. These sample printouts are accompanied by a typical direct path and folded path plot for that turbulence position. Again, each plot includes a header code as described for the printout.

III. EXPERIMENTAL WORK

A. GOALS

There were two main goals for this experiment. First, we wanted to add a component to the existing scintillation measuring system that would allow the introduction of known turbulences along the propagation path in order that the Atmospheric Physics Research Group at the Naval Postgraduate School could investigate various optical propagation phenomena requiring such a component. Secondly, we wanted to compare our experimental results for direct path and folded path scintillation weighting with the theoretical predictions of Ze'evi.

B. PREPARATION

In order to insure proper equipment procedures and to exercise experimental techniques, numerous runs were conducted utilizing the overhead 145 m range in Spanagel Hall. This range is below eight overhead ventillation shafts and is adjoined by many hallway doorways and four building entrances. Thus, there is a great deal of turbulence present but the turbulence was not controllable. No data from these runs are included in the report.

Next we transferred the optics portions of the experiment to the basement floor location of Spanagel where the 61 meter tunnel would be utilized. Practice runs were conducted during

daylight working hours with the tunnel sections open. Again the turbulence was uncontrollable but our runs showed direct path variances in the .014 to .068 range and folded path variances in the range of .018 to .118. These are mentioned only to give some basis by which to compare the quieting effect of our tunnel discussed next. Prior to each experiment we sealed the entire tunnel, sealed all adjoining doorways, and measured a "quiet" tunnel reading that we utilized as our background reading for that experiment. The average quiet tunnel variances for all four experiments were .003 for the direct path laser and .006 for the folded path laser thus giving us reasonable confidence that our tunnel was indeed a region that controlled the turbulence the laser had to propagate through. By subtracting each experiment's respective "quiet" tunnel variance from the individual turbulence position variance during actual runs, we sought to achieve the true effect of the turbulence at that particular position. With these considerations in mind let us now discuss our four experimental runs.

C. FIRST EXPERIMENT - 16 MARCH 1983

For the 16 March 1983 experiment, the equipment setup as described in paragraph II with the following noteworthy ponts. The lens utilized in the direct path setup was a 285 mm plane convex lens set a focal length from the chopper wheel. The turbulence source tunnel section was missing the chimney, roof, and baffle shown in Figure 4. Throughout the run we

attempted to vary the voltage applied to the heating coil to stabilize C_T^2 . Voltages utilized varied from 90 to 105 volts but we failed to truly stabilize C_T^2 . As a result of this problem, we decided to normalize all data for C_T^2 changes. Figures 11 through 14 show the positional variances versus turbulence distance from the detector for this experiment. The solid lines on each graph are the least squares fit of Ze'evi's theoretical path weighting curves. These plot parameters apply to the plots accompanying all four experiments. Detailed data for this run is located in Appendix A.

D. SECOND EXPERIMENT - 27 MARCH 1983

In analyzing the data from the 16 March 1983 run we decided to add the chimney to the tunnel to further isolate the tunnel and turbulence source from the possibility that hallway breezes may have introduced fluctuations in the turbulence presented to the lasers during propagation. Additionally, we realized the interference patterns we observed on the detector face for the direct path and folded path patterns may have influenced our readings. To eliminate these interference patterns, great care was taken to eliminate the reflections off the back face of the splitters. The folded path interference pattern was eliminated by intercepting the secondary beam off the back face of the folded path splitter with a small wooden stick. Careful examination of the beam structure at the target mirror and on the detector face indicated that this eliminated the interference problem without introducing structure to the beam.

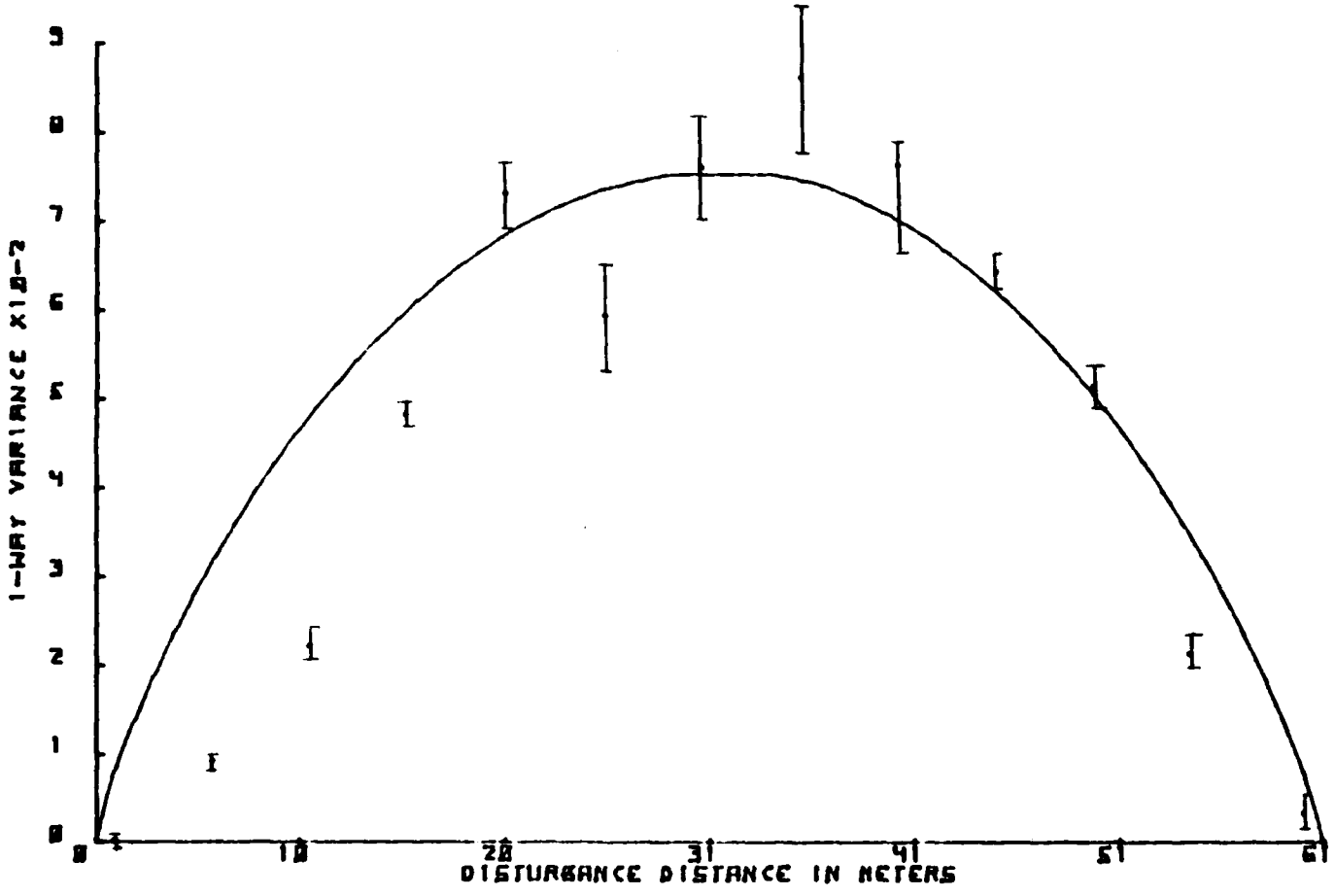

Figure 11. Plot of the Direct Path (one-way) Variance Versus Disturbance Distance from the Detector for the 16 March 1983 Experiment. The solid line represents the least squares fit of Ze'evi's prediction.

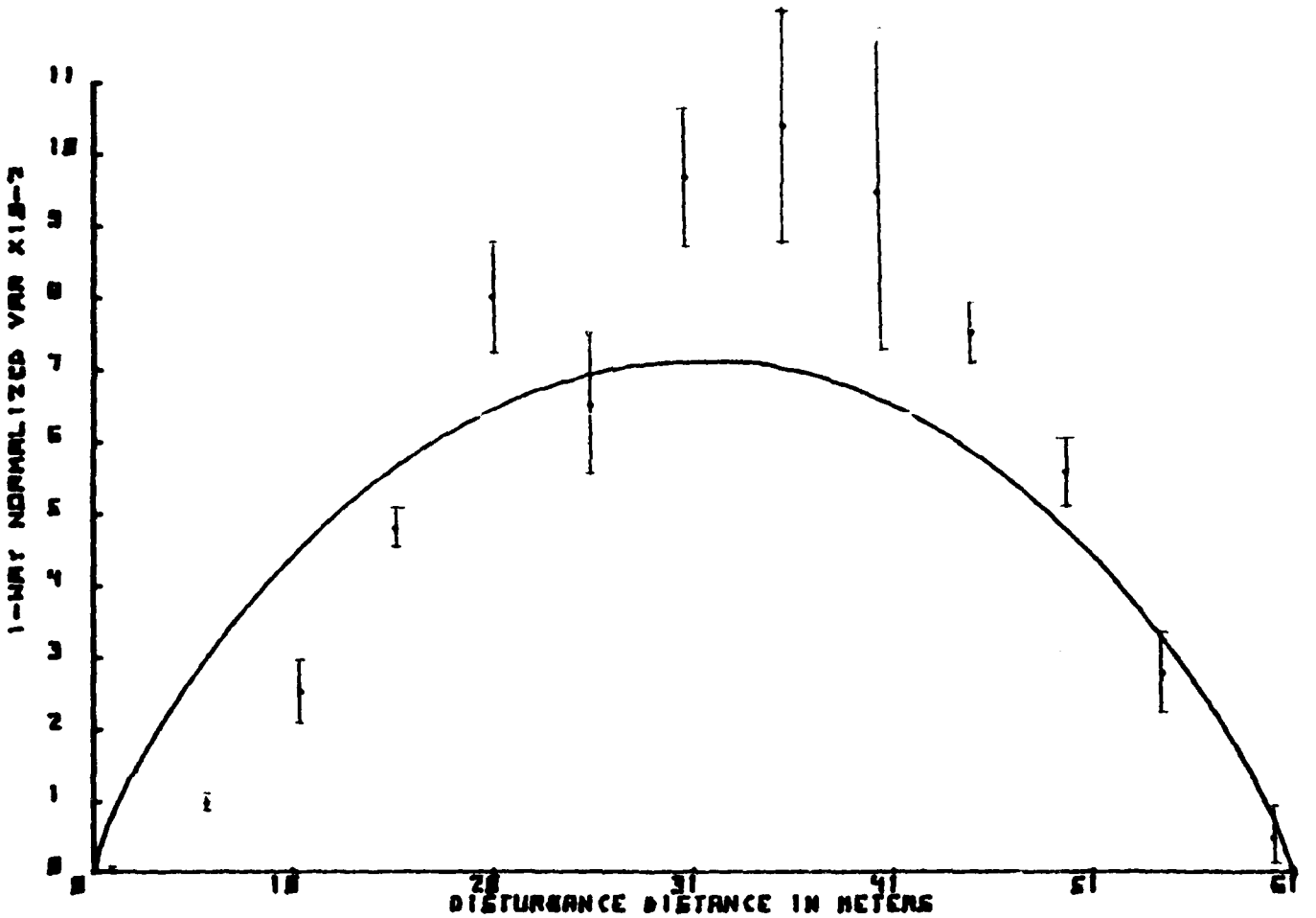

Figure 12. Plot of the Normalized Direct Path (one-way) Variance Versus Distance from the Detector for the 16 March 1983 Experiment. Data was normalized for C_T^2. Solid line represents the least square fit of Ze'evi's prediction.

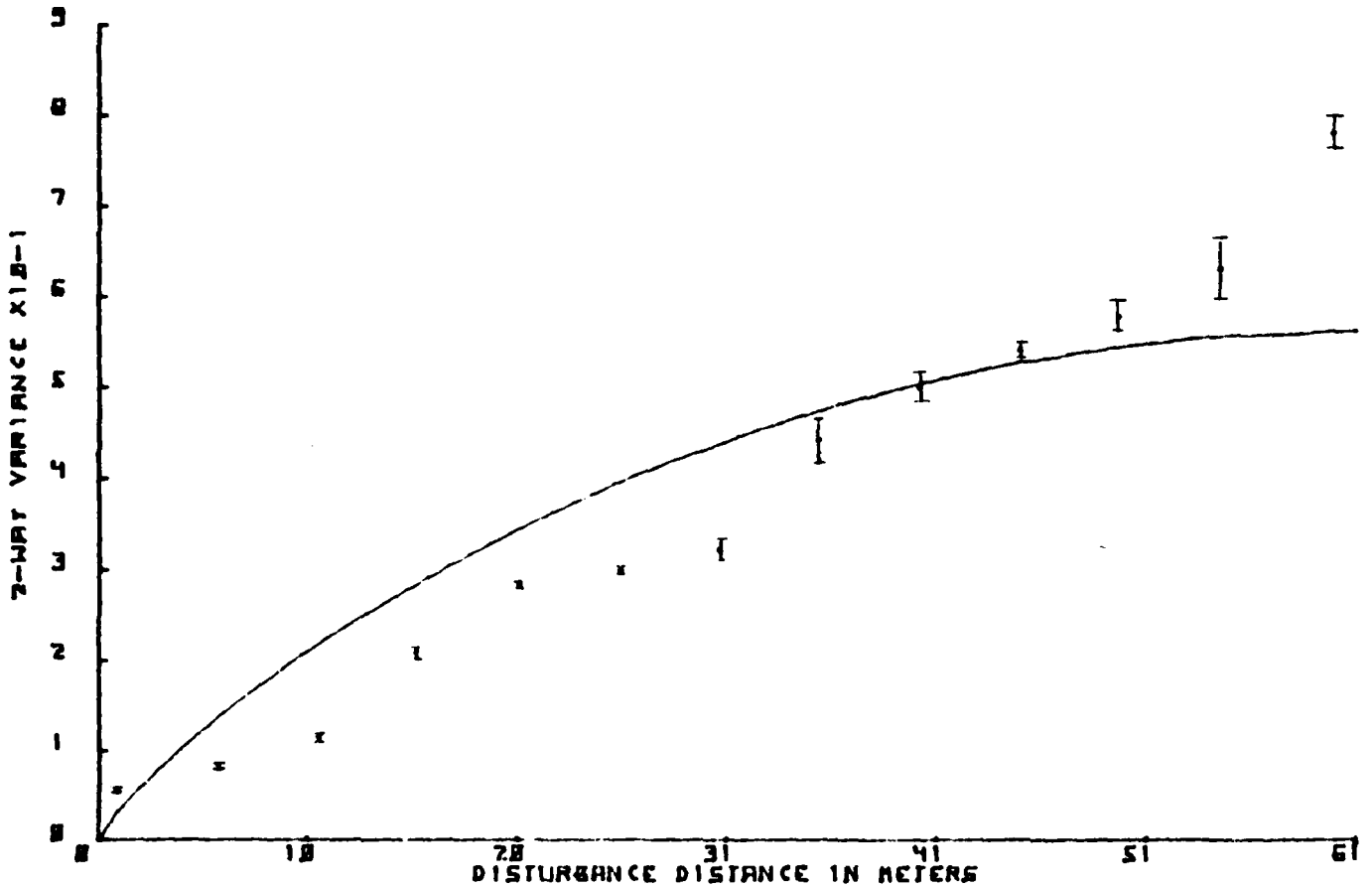

Figure 13. Plot of the Folded Path (two-way) Variance Versus Disturbance Distance from the Detector for the 16 March 1983 Experiment. The solid line represents the least square fit of Ze'evi's prediction.

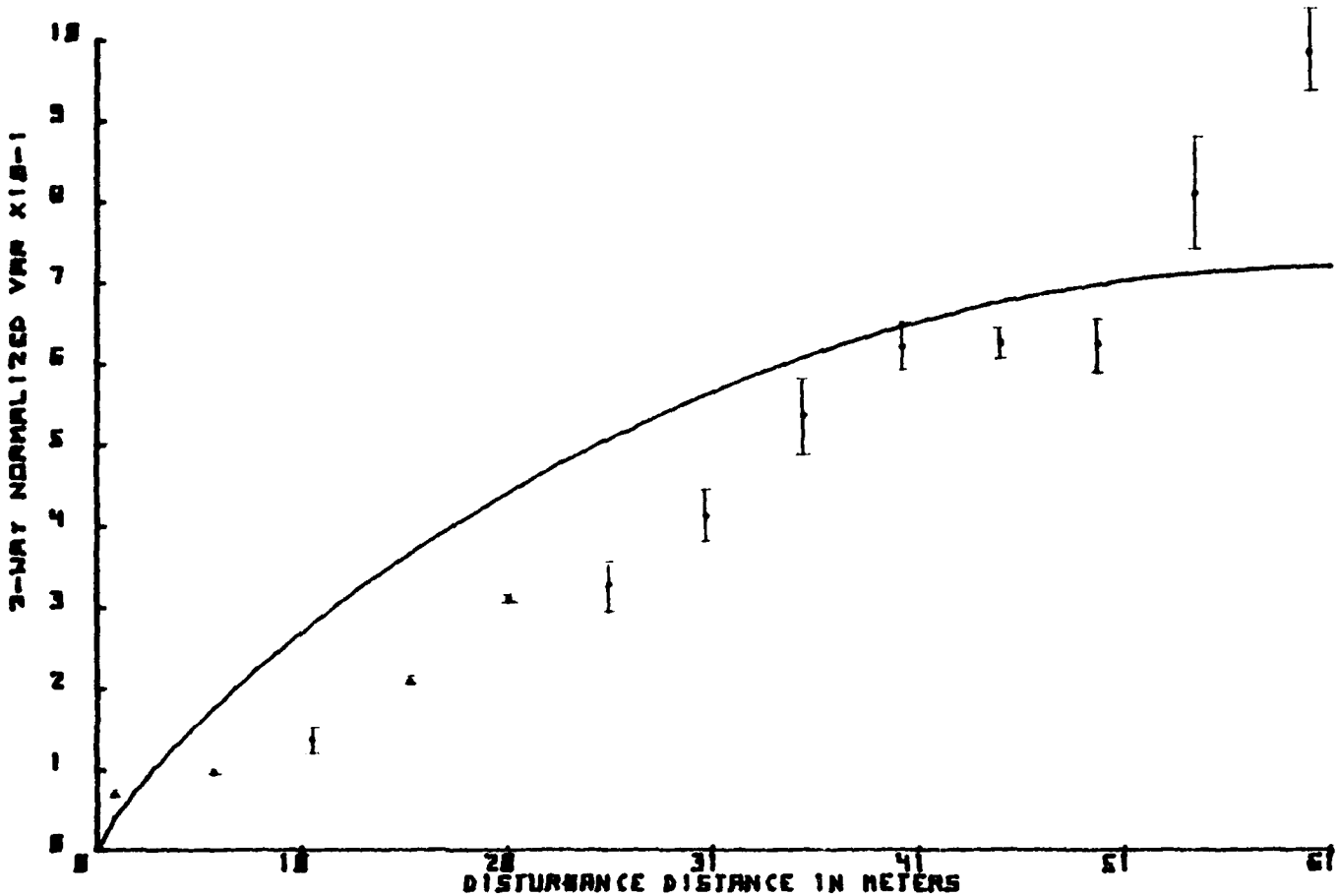

Figure 14. Plot of the Normalized Folded Path Variance Versus Disturbance Distance from the Detector for the 16 March 1983 Experiment. Data was normalized for C_T^2. Solid line represents the least square fit of Ze'evi's prediction.

The direct path pattern was eliminated by removing the 285 mm lens and properly orienting the polarizers and direct path splitter to achieve the Brewster angle. This eliminated the interference pattern but in analyzing the results of this experiment we realized that we had introduced and measured beam wander as a result of too narrow a beam in the portion of the tunnel near the direct path splitter. However, the folded path data for the run was valid and the variance and normalized variance plots are presented in Figures 15 and 16. Detailed data for the 27 March 1983 run is presented in Appendix B.

E. THIRD EXPERIMENT - 30 MARCH 1983

To eliminate the beam wander and interference pattern problem for the direct path laser we introduced a 10 cm focal length convex-convex lens as our lens before the chopper. This gave us a large uniformly structured beam at the aperture for our third experiment. Additionally we decided to lower the heater voltage to 70 volts for this run and to leave the voltage constant throughout the experiment. The plots of the variances versus distrubance distance for this experiment are presented in Figures 17 through 20. Detailed data for this run is located in Appendix C.

F. FOURTH EXPERIMENT - 13 APRIL 1983

In analyzing the data of 30 March 1983 we decided to add the roof and baffle to the turbulence source tunnel to better isolate the turbulence source from the hallway environment.

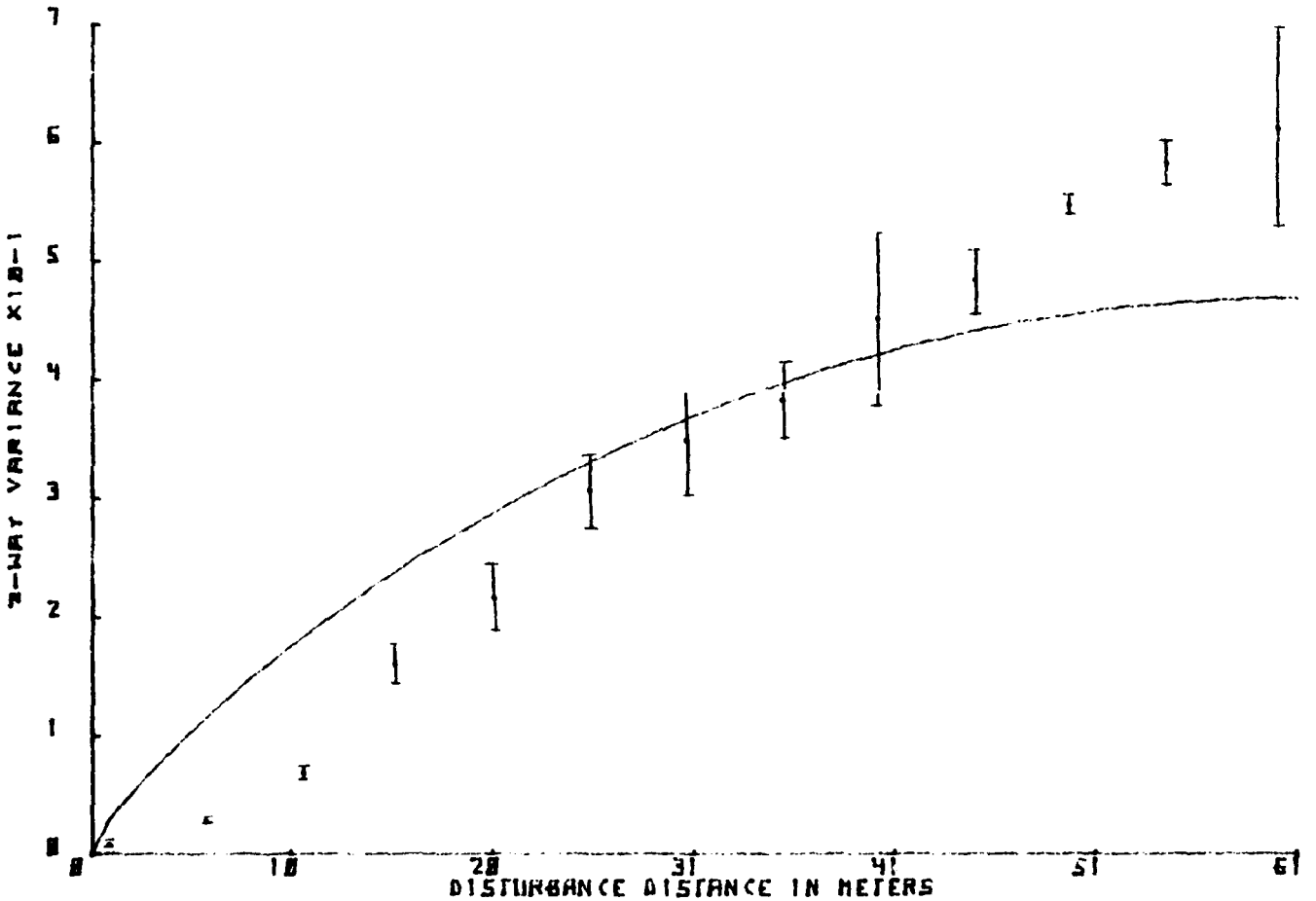

Figure 15. Plot of Folded Path (two-way) Variance Versus Disturbance Distance from the Detector for the 27 March 1983 Experiment. Solid line represents the least squares fit of Ze'evi's prediction.

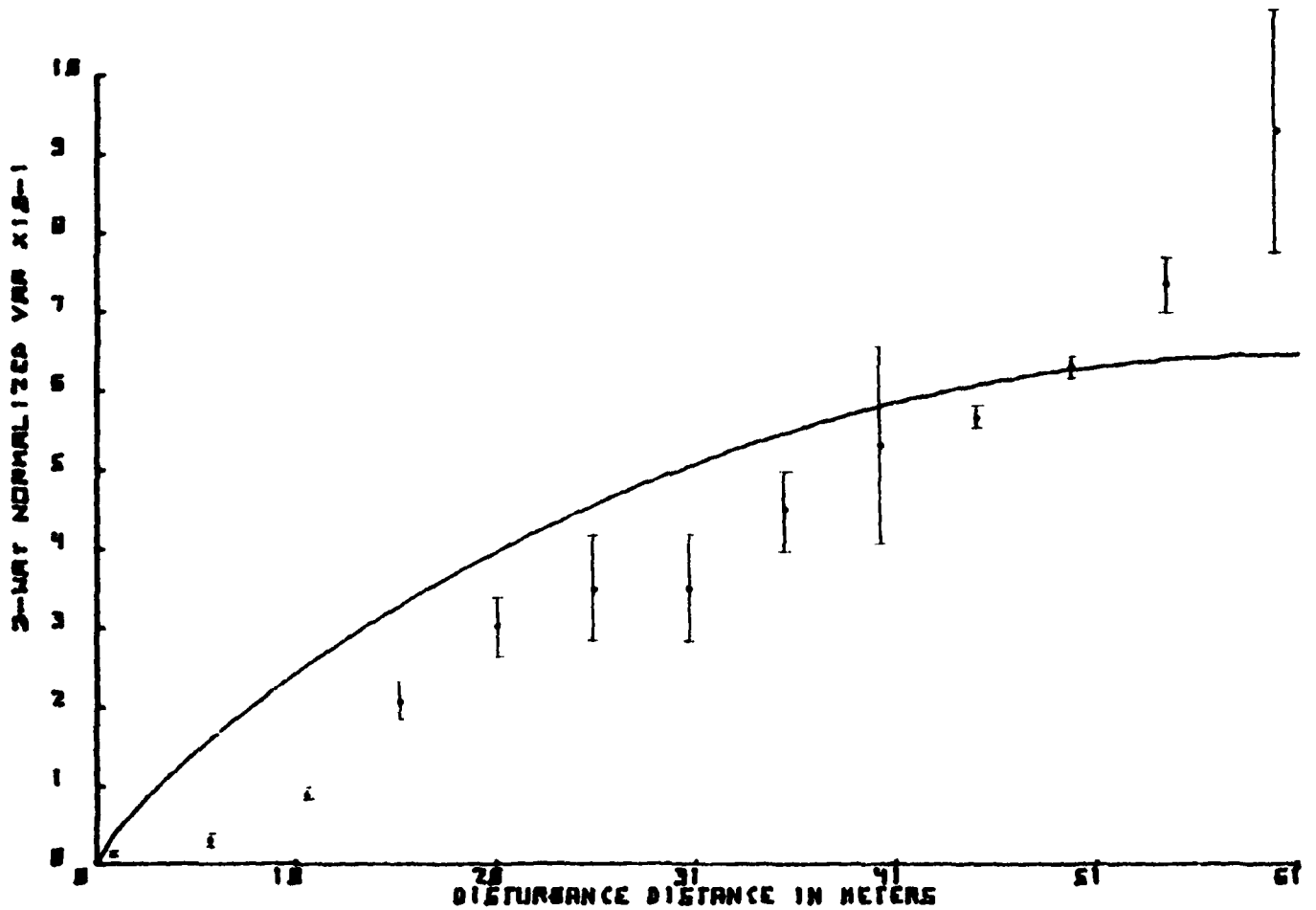

Figure 16. Plot of Normalized Folded Path (two-way) Variance Versus Disturbance Distance from the Detector for the 27 March 1983 Experiment. Data was normalized for C_T^2. Solid line represents the least squares fit of Ze'evi's prediction.

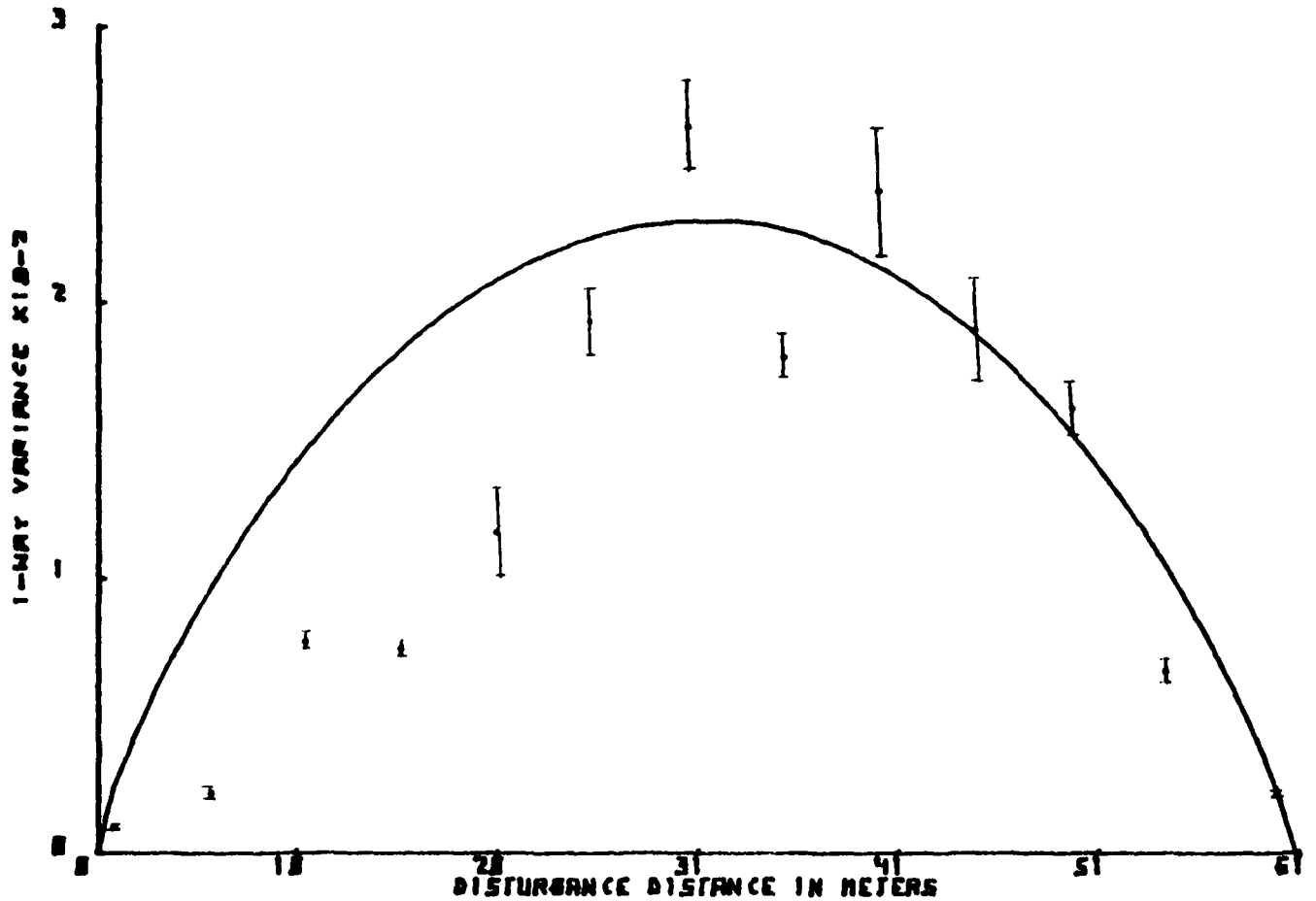

Figure 17. Plot of Direct Path (one-way) Variance Versus Disturbance Distance from the Detector for the 30 March 1983 Experiment. The solid line represents the least squares fit of Ze'evi's prediction.

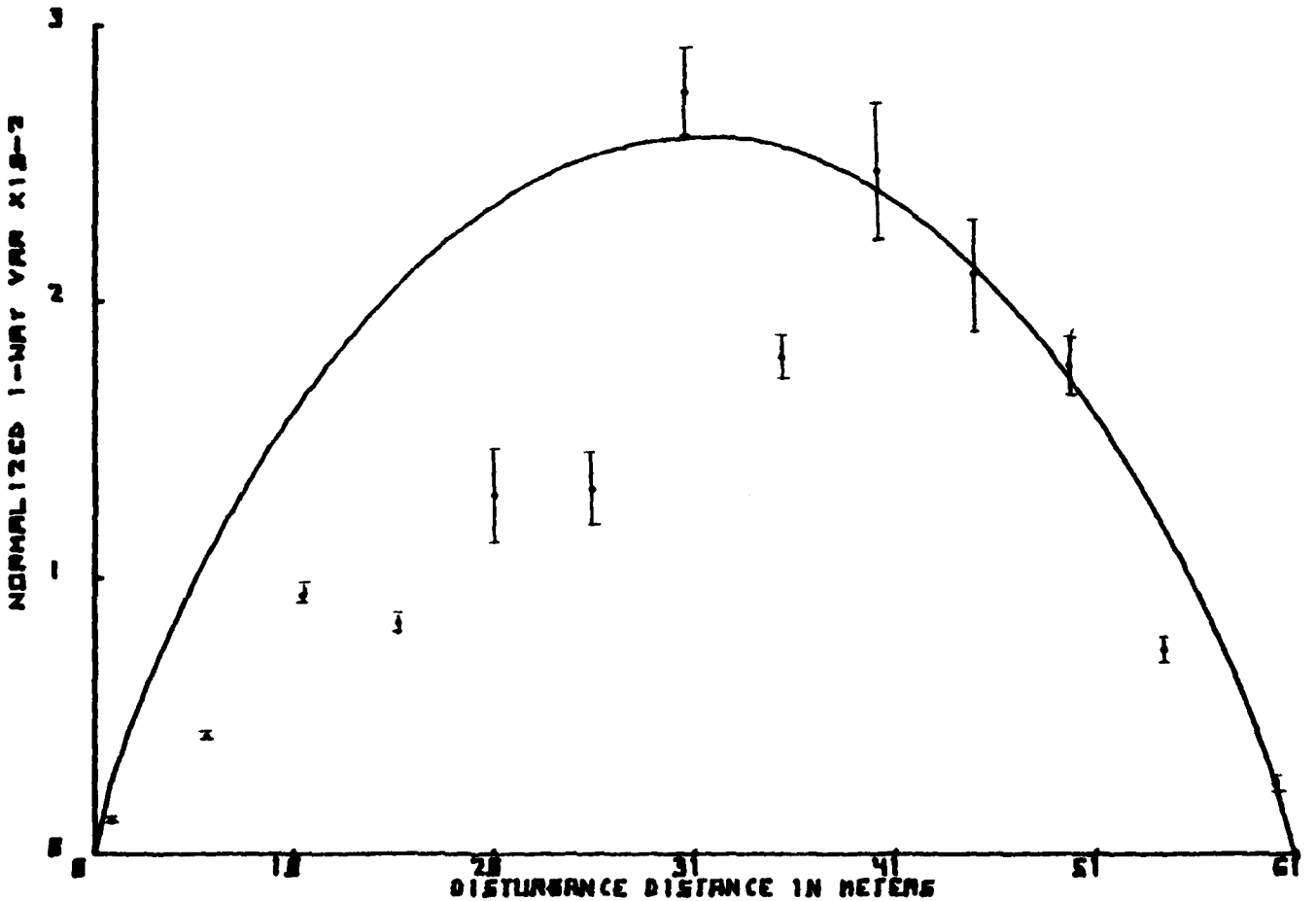

Figure 18. Plot of Normalized Direct Path (one-way) Variance Versus Disturbance Distance from the Detector for the 30 March 1983 Experiment. Data was normalized for C_T^2. Solid line represents the least squares fit of Ze'evi's prediction.

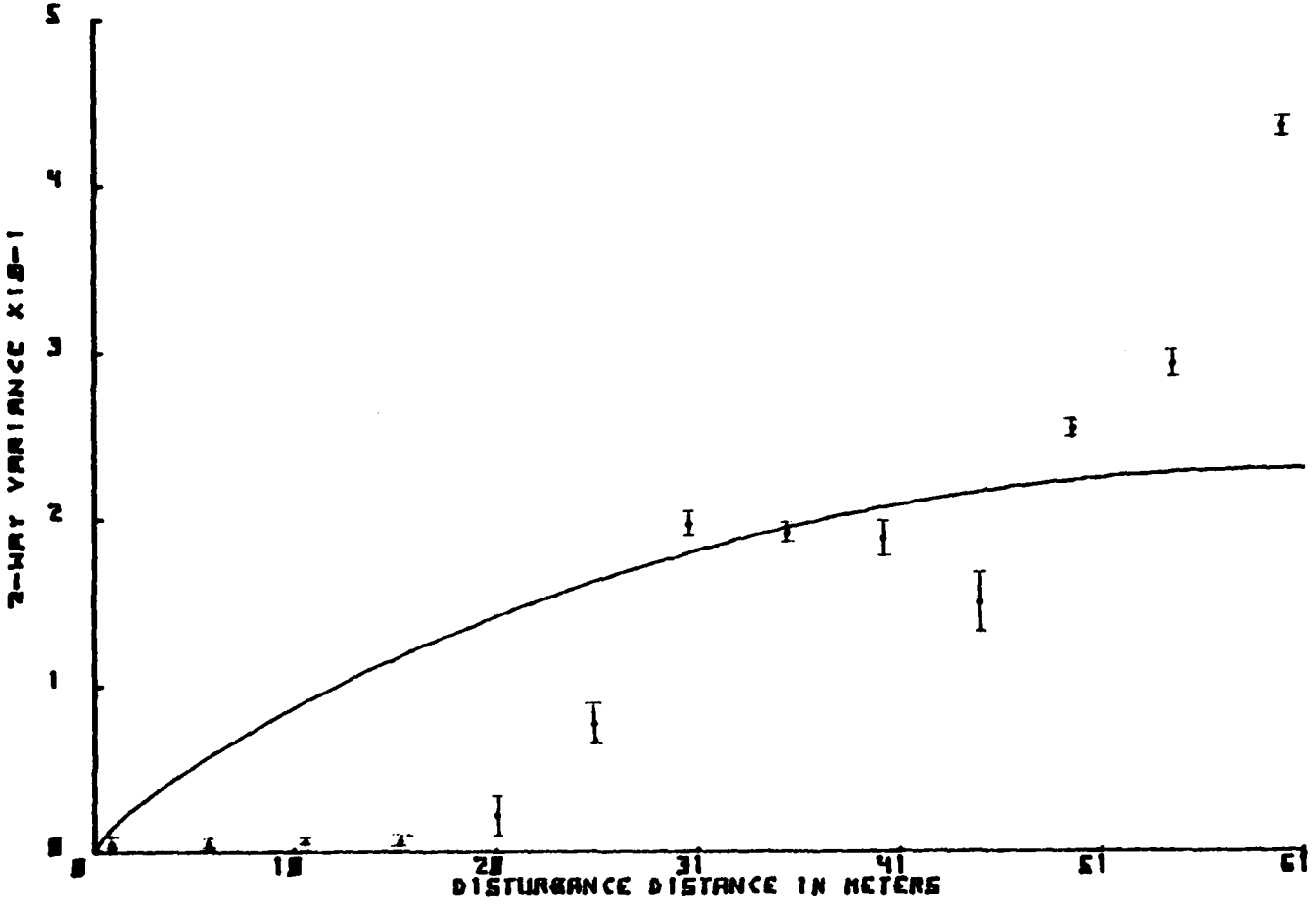

Figure 19. Plot of Folded Path (two-way) Variance Versus Disturbance Distance from the Detector for the 30 March 1983 Experiment. Solid line represents the least squares fit of Ze'evi's prediction.

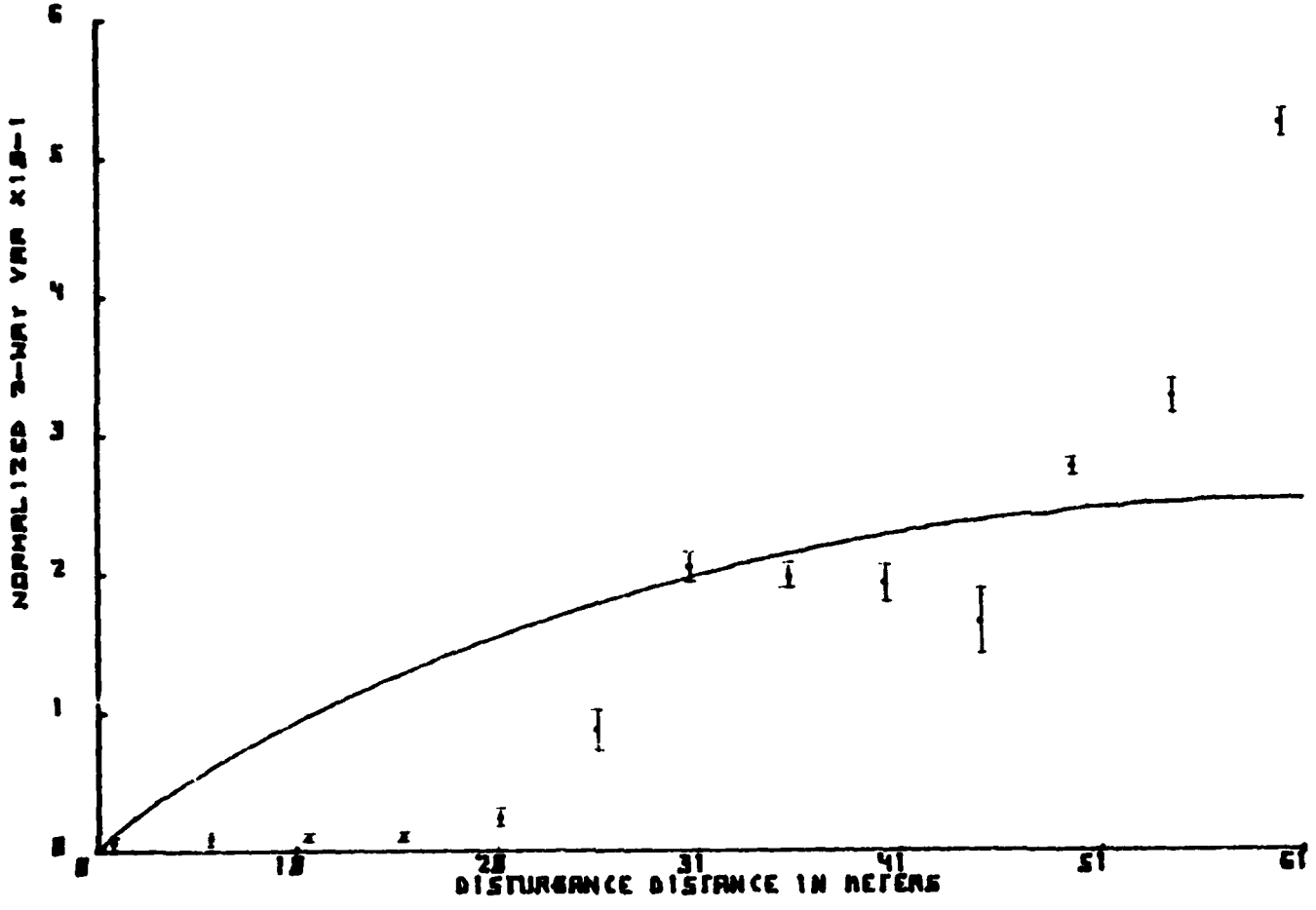

Figure 20. Plot of Normalized Folded Path (two-way) Variance Versus Disturbance Distance from the Detector. Data was normalized for C_T^2. Solid line represents the least squares fit of Ze'evi's prediction. Experiment was conducted 20 March 1983.

We feared that air from an overhead vent or cooler air from building stairwells may have directly entered the heater. Additionally, realizing that the results we had received thus far showed a consistent pattern of less weighting at the detector end for both sources and greater weighting at the target end for the folded path laser than predicted by Ze'evi we decided to reverse the optics locations in the hallway to insure that our results were not dependent on a particular hallway configuration. The plots of variances versus disturbance location from the detector are presented in Figures 21 through 24. It is significant to note that reversing the optics did not change the overall path weighting pattern we previously encountered. Detailed statistics of the 13 April 1983 run are located in Appendix D.

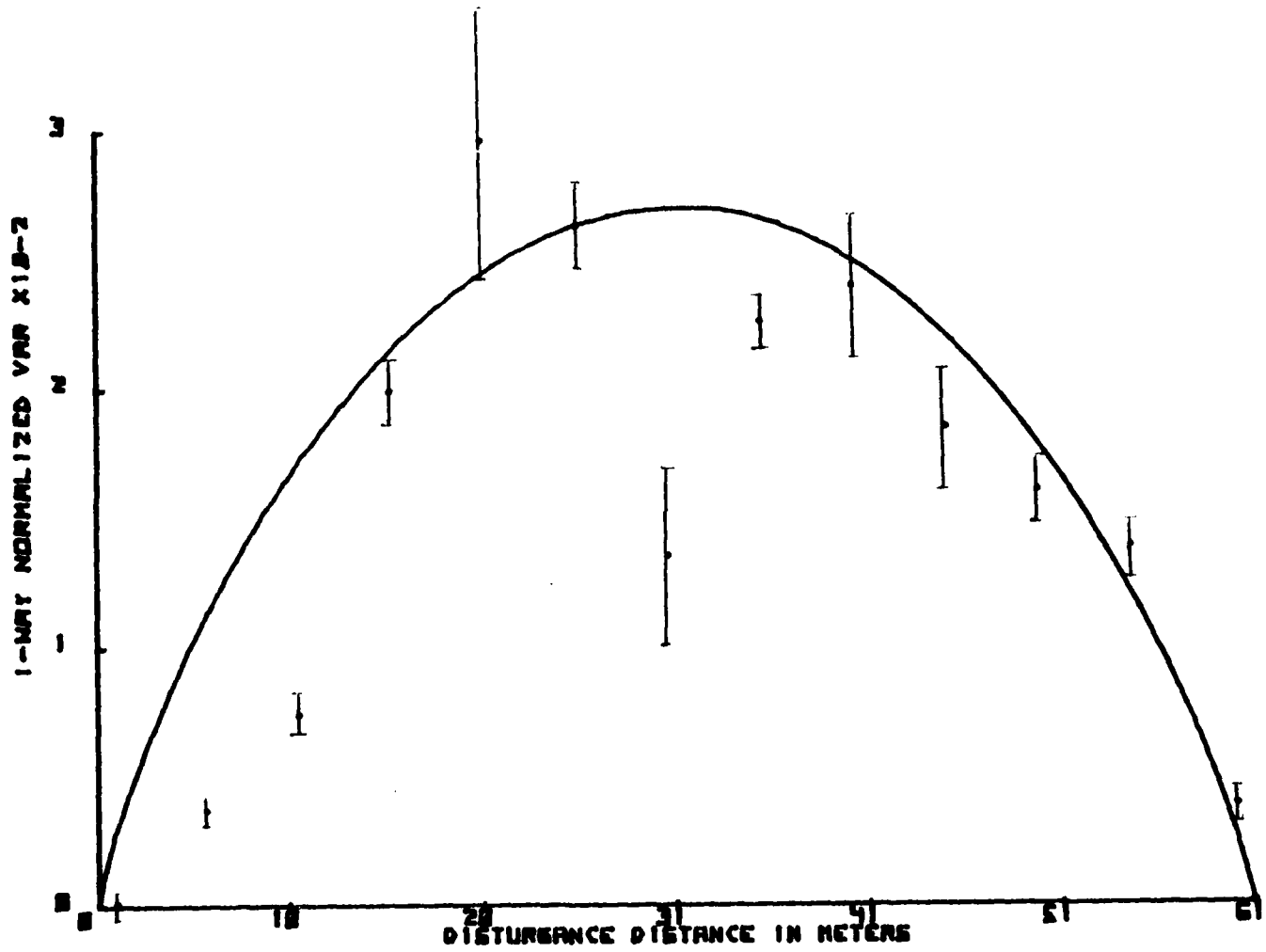

Figure 21. Plot of Direct Path (one-way) Variance Versus Disturbance Distance from Detector for the 13 April 1983 Experiment. Solid line represents the least squares fit of Ze'evi's prediction.

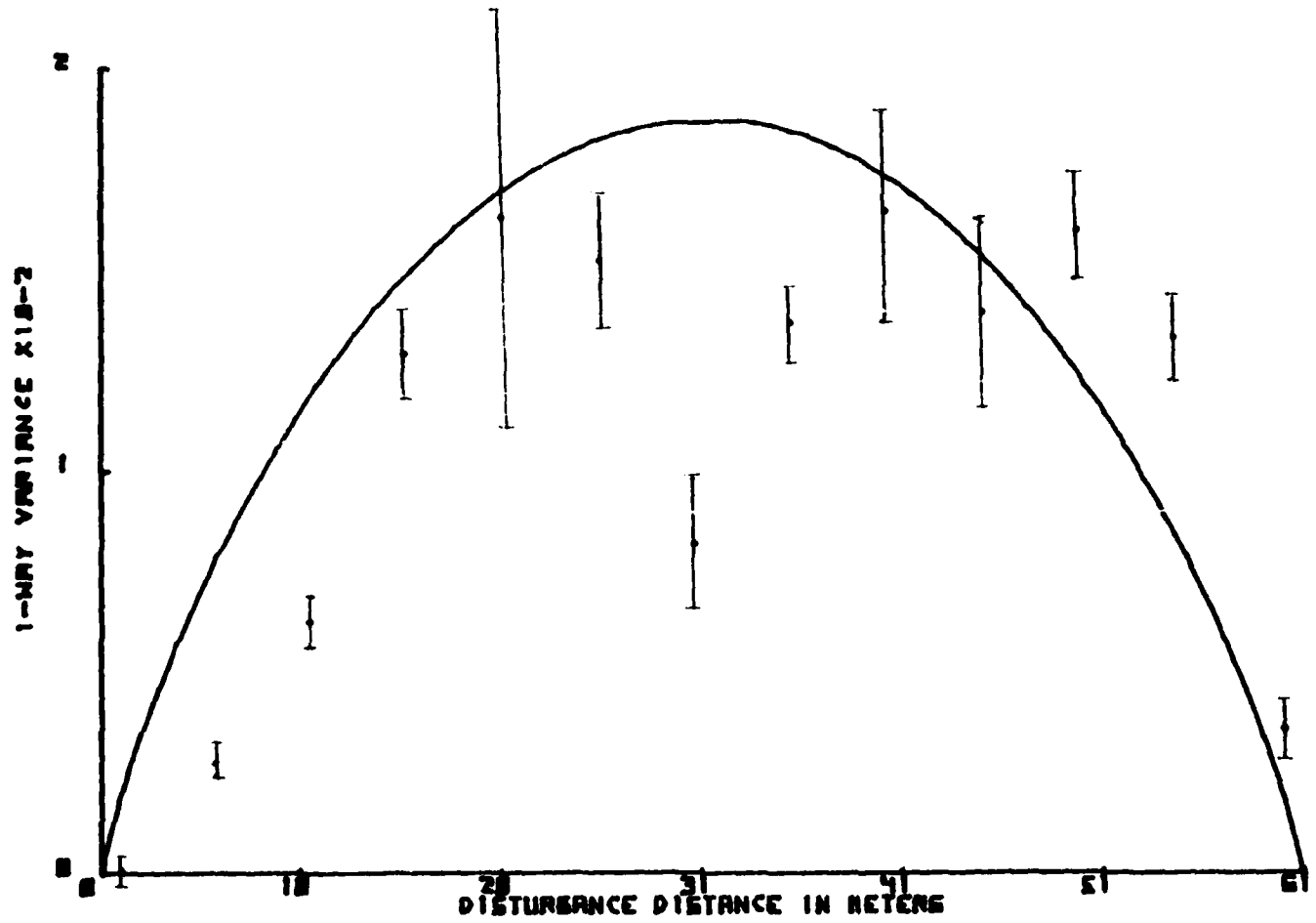

Figure 22. Plot of Normalized Direct Path (one-way) Variance Versus Disturbance Distance from the Detector for the 13 April 1983 Experiment. Data was normalized for C_T^2. Solid line represents the least squares fit of Ze'evi's prediction.

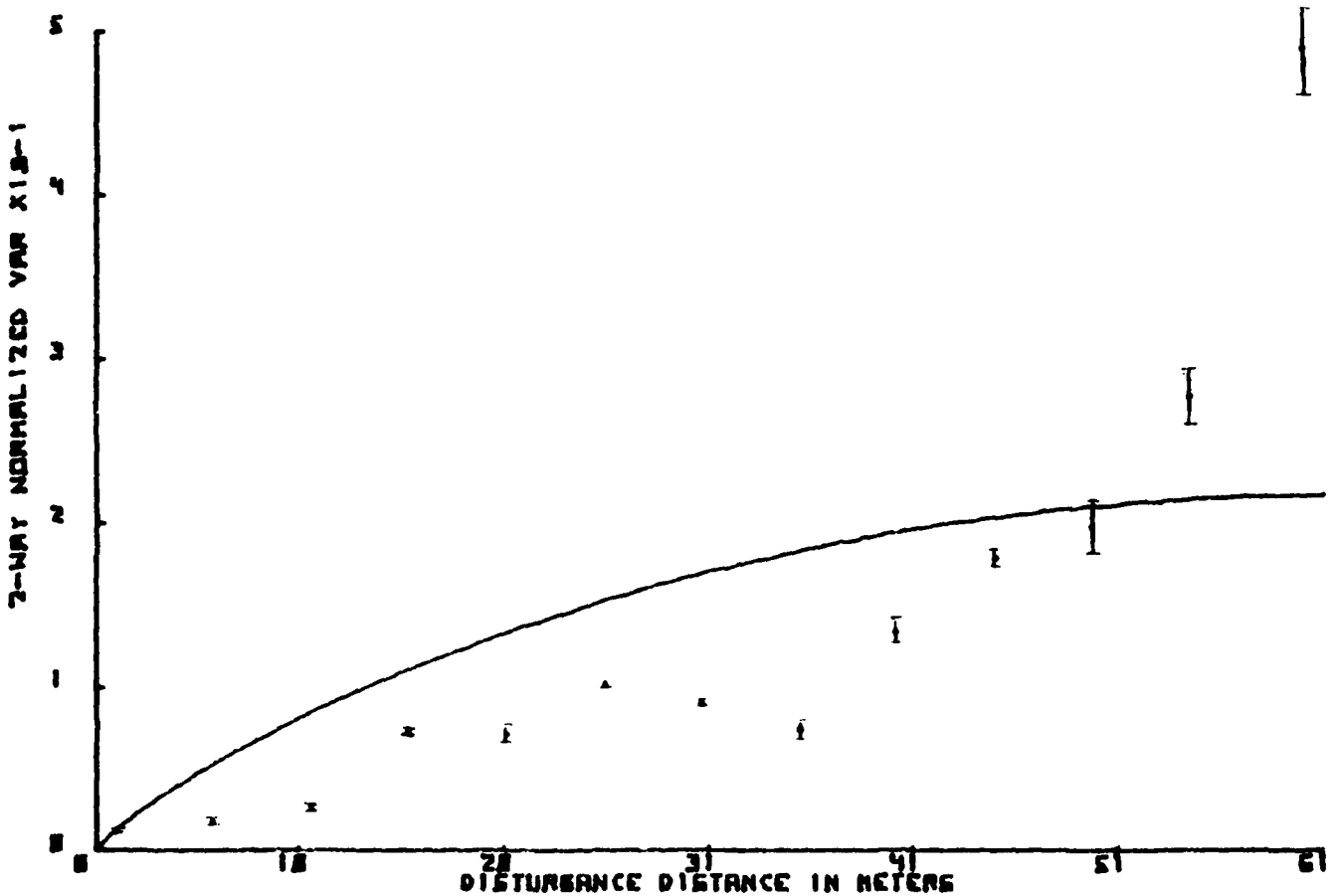

Figure 23. Plot of Folded Path (two-way) Variance Versus Disturbance Distance from the Detector for the 13 April 1983 Experiment. Solid line represents the least squares fit of Ze'evi's prediction.

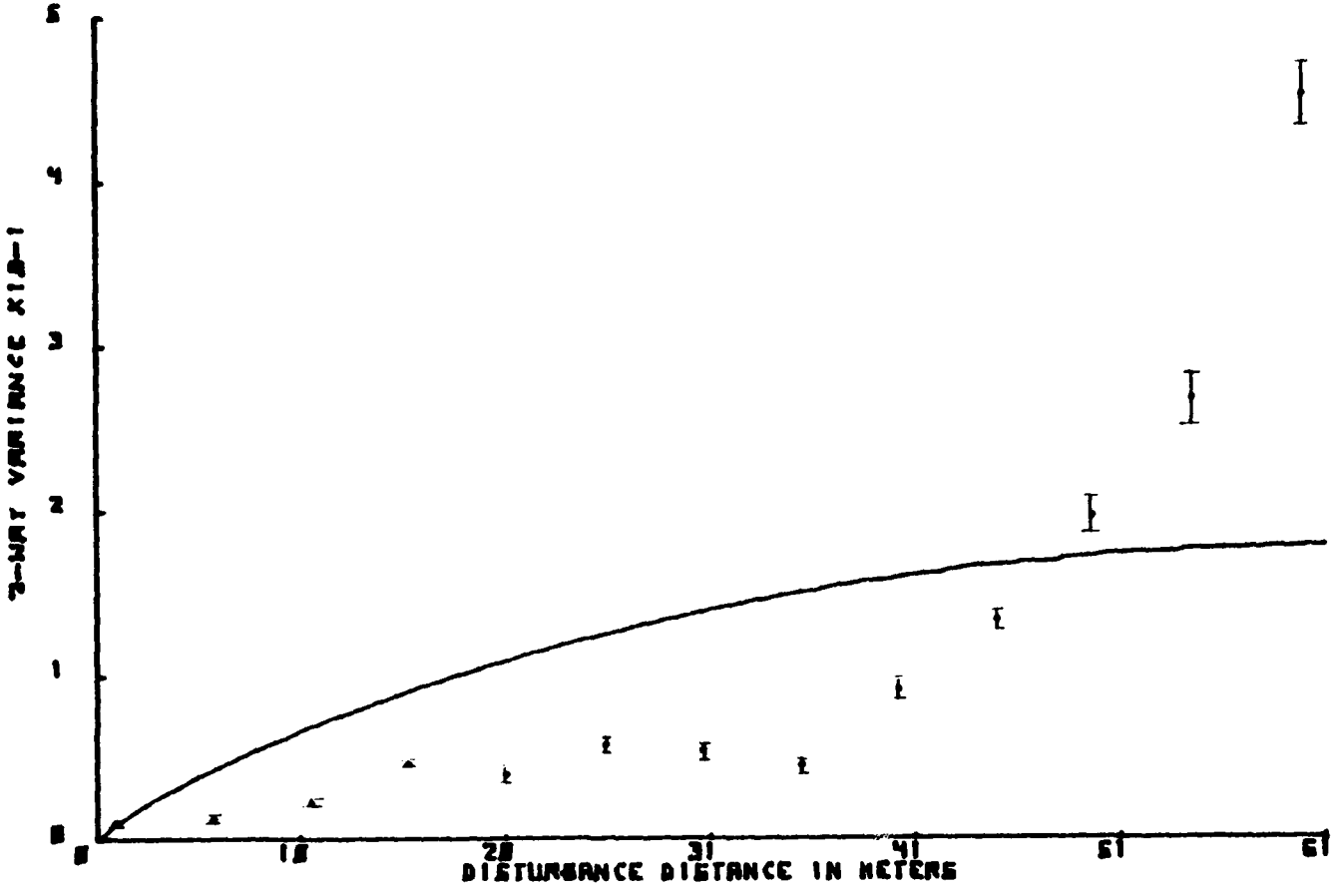

Figure 24. Plot of Normalized Folded Path (two-way) Variance Versus Disturbance Distance from the Detector for the 13 April 1983 Experiment. Data was normalized for C_T^2. Solid line represents the least squares fit of Ze'evi's prediction.

IV. CONCLUSIONS

A. FINDINGS

Based upon our experimental results and data analysis we state the following findings:

1. In examining our four experimental runs we conclude that the data we obtained follows the general pattern of Ze'evi's prediction but fails to conform exactly to his predicted path weighting. In particular, our data indicates a lower path weighting in the vicinity of the detector for both the direct path and folded path and that a much more severe path weighting in the vicinity of the target mirror existed than Ze'evi predicted.

2. Our experiments were conducted in the low turbulence region defined by $\sigma_\ell^2 \tilde{<} 1$. The actual σ_ℓ^2 measured were generally less than .9. In examining our chi-square values for these distributions we must conclude that in the turbulence region of our experiment the log intensity distribution was not a true Gaussian distribution since our chi-square goodness of fit parameters generally exceeded the established value of 288.87 for a 95% confidence interval.

3. We state with confidence that the turbulence chamber setup utilized was an acceptable method for introducing a known turbulence in the laser propagation paths and that run number four demonstrated that our findings are independent of the terminal optics locations with respect to the hallway configuration.

4. A closer examination of the folded path variance versus disturbance distance indicated that a complicated three region pattern may actually exist. This may be worthy of further examination.

5. As we attempted to refine our experiment and believed we understood more about what was actually happening along the propagation path, we began to fully realize that unpredictable scintillation effects could occur at any time. As an example we could not explain the unusual dip in the direct path variance for the 30.1 meter position in our last run.

B. FUTURE WORK

Future work utilizing the system as currently configured could include:

1. Repetition of the current experiment to build a large data base may be considered in order to aid in ascertaining a path weighting formula that more accurately predicts the empirical data.

2. The use of the turbulence chamber to attempt to verify Ze'evi's predicted correlation of direct and folded path scintillation for small angles other than the exact folded path ($\theta = 0$) would be of interest.

3. Use of a corner cube reflector and other specular reflectors for the folded path target and the examination of the scintillation path weighting for such setups would be of value to many currently applied uses of lasers utilizing folded paths.

DIRECT PATH SCINTILLATION DATA - 16 MARCH 1983

Disturbance Distance (Meters)	$\langle\sigma_i\rangle$	$(\langle\sigma_i\rangle^2 - \langle\sigma\rangle^2_{quiet}) \times 10^{-2}$	$C_T^2 (K^2/m^{-2/3})$	$(\langle\sigma_i\rangle^2 - \langle\sigma\rangle^2_{quiet}) \times 10^{-2}$ Normalized for C_T^2
Quiet	.0577 ± .0018			
1.0	.0486 ± .0005	.0962 ± .039	218.27	0 ± .089
5.8	.1088 ± .0009	.8514 ± .029	242.53	.9493 ± .105
10.7	.1579 ± .0056	2.161 ± .178	234.55	2.491 ± .456
15.5	.2258 ± .0028	4.764 ± .128	270.41	4.764 ± .285
20.4	.2760 ± .007	7.284 ± .387	247.04	7.973 ± .769
25.3	.2502 ± .012	5.925 ± .601	248.42	6.450 ± 1.238
30.1	.2813 ± .010	7.581 ± .563	212.80	9.633 ± 1.109
35.0	.2981 ± .014	8.554 ± .835	223.39	10.354 ± 1.607
39.8	.2820 ± .020	7.619 ± .113	219.21	9.398 ± 2.215
44.7	.2603 ± .004	6.441 ± .209	234.51	7.427 ± .430
49.5	.2337 ± .005	5.129 ± .235	252.16	5.500 ± .503
54.4	.1566 ± .007	2.121 ± .220	211.30	2.714 ± .564
60.0	.0812 ± .006	3.266 ± .100	214.73	.4113 ± .353

FOLDED PATH SCINTILLATION DATA - 16 MARCH 1983

Disturbance Distance (Meters)	$\langle\sigma_i\rangle$		$(\langle\sigma_i\rangle^2 - \langle\sigma\rangle^2_{quiet}) \times 10^{-1}$		$C_T^2 (K^2/m^{-2/3})$	$(\langle\sigma_i\rangle^2 - \langle\sigma_{quiet}\rangle^2) \times 10^{-1}$ Normalized for C_T^2	
Quiet	.0663	± .004					
1.0	.2344	± .0049	.5465	± .0054	218.27	.6771	± .0518
5.8	.3017	± .033	.8681	± .0060	242.53	.9679	± .0548
10.7	.3472	± .0130	1.1061	± .0313	234.55	1.3376	± .1560
15.5	.4613	± .0046	2.0843	± .0195	270.41	2.0843	± .0682
20.4	.5358	± .0015	2.8269	± .0086	247.04	3.0954	± .0989
25.3	.5521	± .020	3.0036	± .0003	248.42	3.2710	± .2979
30.1	.5721	± .0177	3.2293	± .1158	212.80	4.1045	± .2991
35.0	.6681	± .022	4.4200	± .1964	223.39	5.3481	± .4449
39.8	.7104	± .016	5.0024	± .1614	219.21	6.1729	± .3165
44.7	.7387	± .009	5.4132	± .0982	234.51	6.2419	± .1885
49.5	.7631	± .013	5.7785	± .15138	252.16	6.1945	± .3240
54.4	.7967	± .027	6.3026	± .3427	211.30	8.0673	± .7272
60.0	.8849	± .015	7.7856	± .2348	214.73	9.8021	± .5018

MAR. 16 1983
AP,370,.03,300K,0
1820,QUIET
Wavelength= 6.33E-07 meters

Scintillation measurements or Sigma
16384 samples for eacn measurement
Fixed range= 61 meters

# pts	Sigma	Chi Square
1:16384	0.0542	7.24E 01
1:16384	0.0639	1.53E 02
2:16385	0.0556	1.06E 02
2:16383	0.0617	1.09E 02
3:16385	0.0566	9.51E 01
3:16383	0.0637	1.30E 02
4:16385	0.0636	7.05E 01
4:16383	0.0640	1.05E 02

Figure 25. Scintillation Statistics

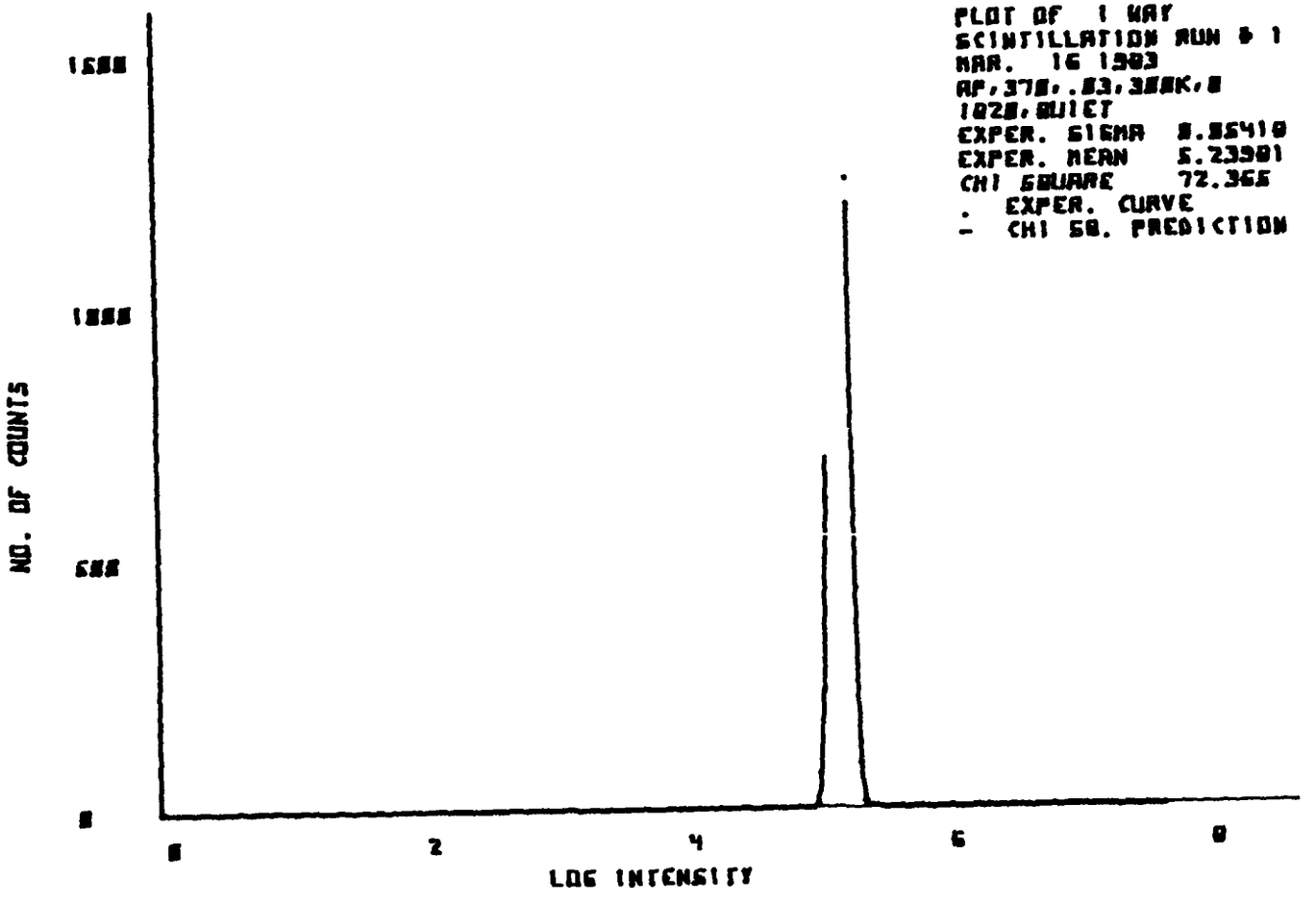

Figure 26. Scintillation Data and Theoretical Curve

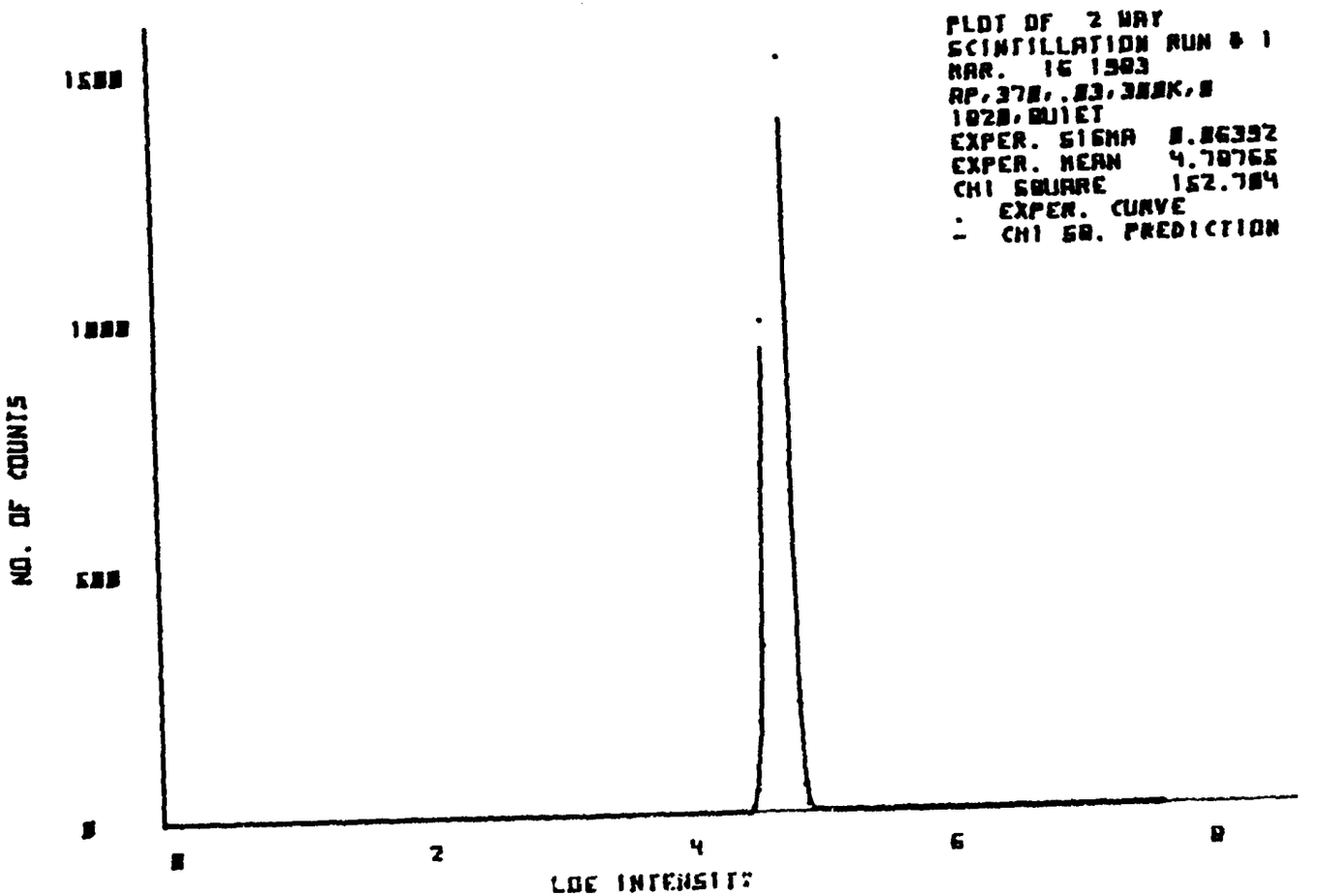

Figure 27. Scintillation Data and Theoretical Curve

```
MAR.  16 1983
AP,370,.03,300K,0
2200,20.4m
wavelength=    6.33E-07 meters


Scintillation measurements of Sigma
16384 samples for each measurement
Fixed range=     61 meters

    # pts          Sigma      Chi Square

   1:16384        0.2710     1.24E 03**
   1:16384        0.5316     7.66E 02**
   2:16383        0.2636     1.18E 03**
   2:16385        0.5400     6.65E 02**
   3:16383        0.2942     1.05E 03**
   3:16385        0.5373     9.37E 02**
   4:16383        0.2557     1.72E 02
   4:16385        0.5343     5.66E 02**
```

Figure 28. Scintillation Statistics

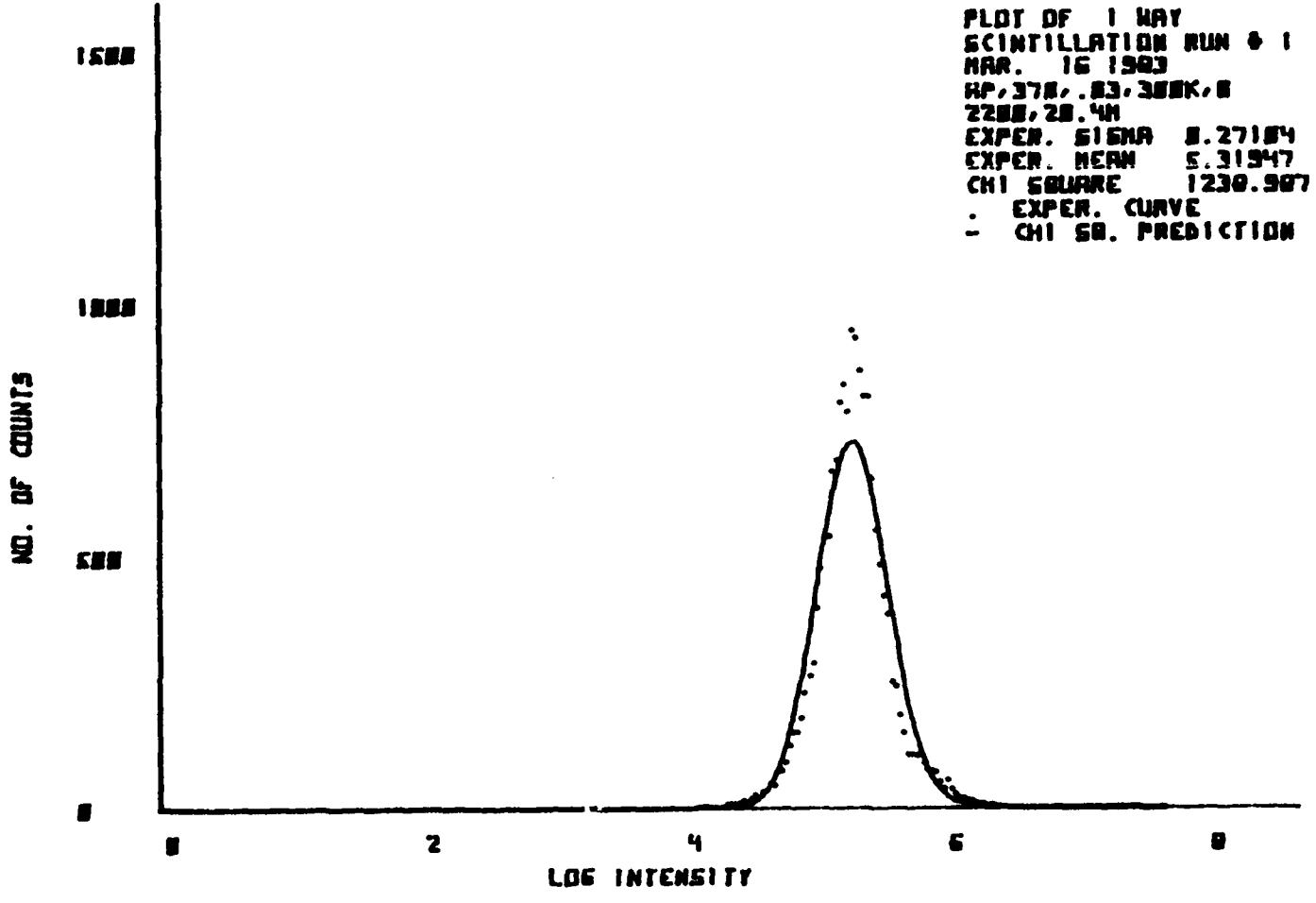

Figure 29. Scintillation Data and Theoretical Curve

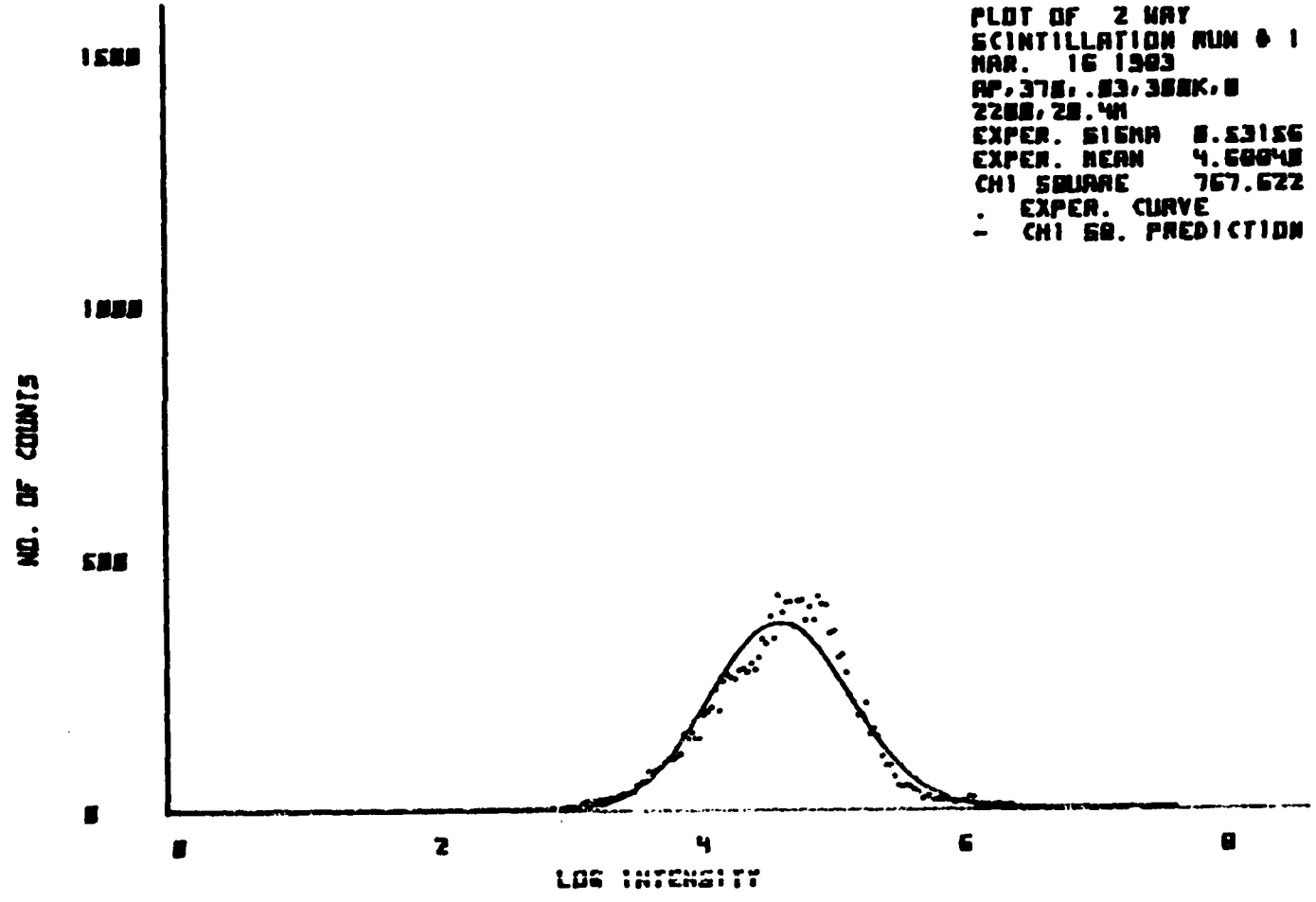

Figure 30. Scintillation Data and Theoretical Curve

```
MAR.  17 1983
AP,370,.3,10K,0
0300,60m
wavelength=    0.33E-07 meters


Scintillation measurements or Sigma
16384 samples for each measurement
Fixed range=    61 meters

    # pts        Sigma     Chi Square

   1:16384      0.0818    1.37E 02
   1:16349      0.8454    7.15E 02**
   2:16383      0.0819    6.74E 02**
   2:16362      0.8919    5.86E 02**
   3:16383      0.0789    1.60E 02
   3:16355      0.8762    7.97E 02**
   4:16383      0.0821    3.50E 02**
   4:16336      0.9259    7.00E 02**
```

Figure 31. Scintillation Statistics

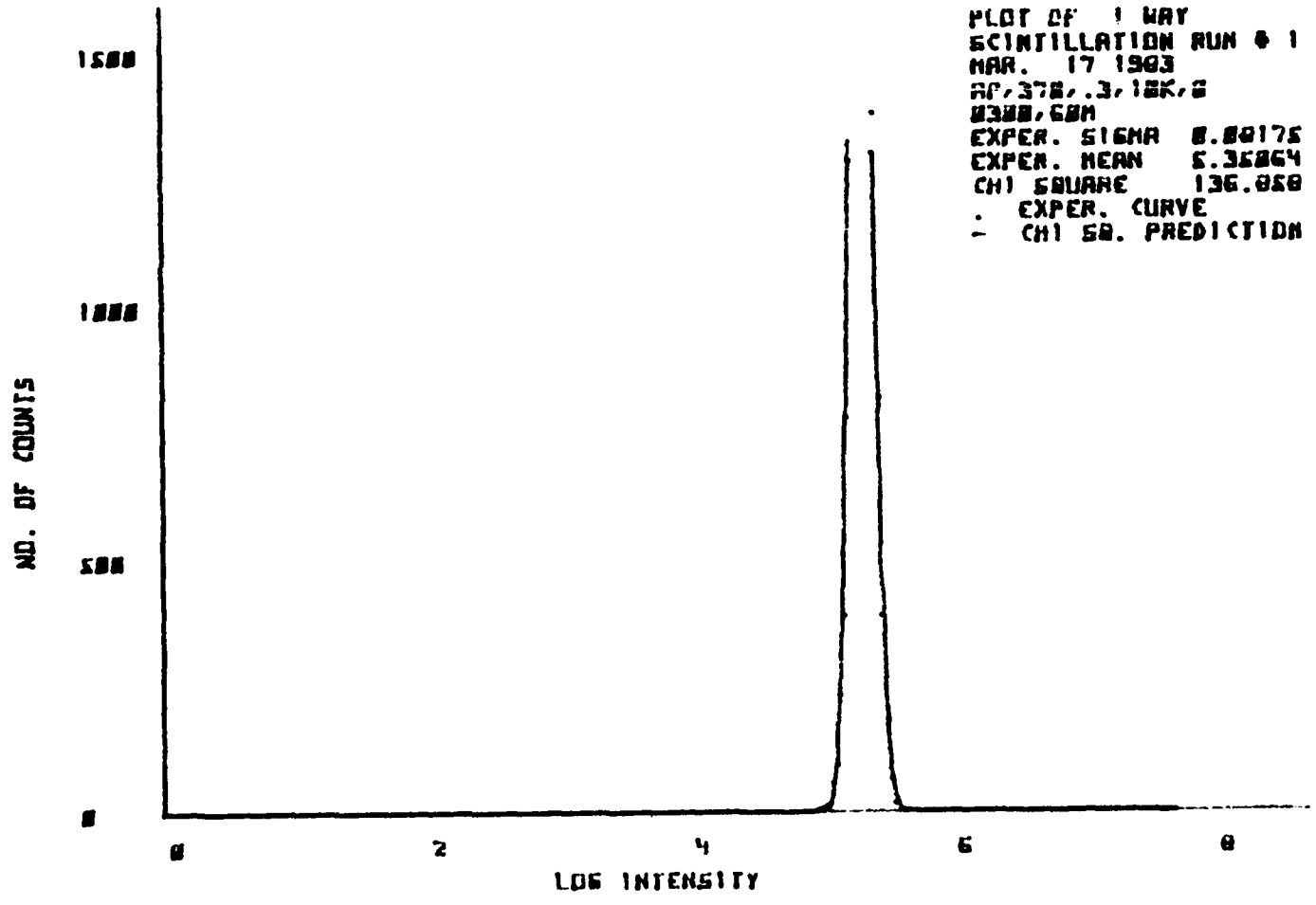

Figure 32. Scintillation Data and Theoretical Curve

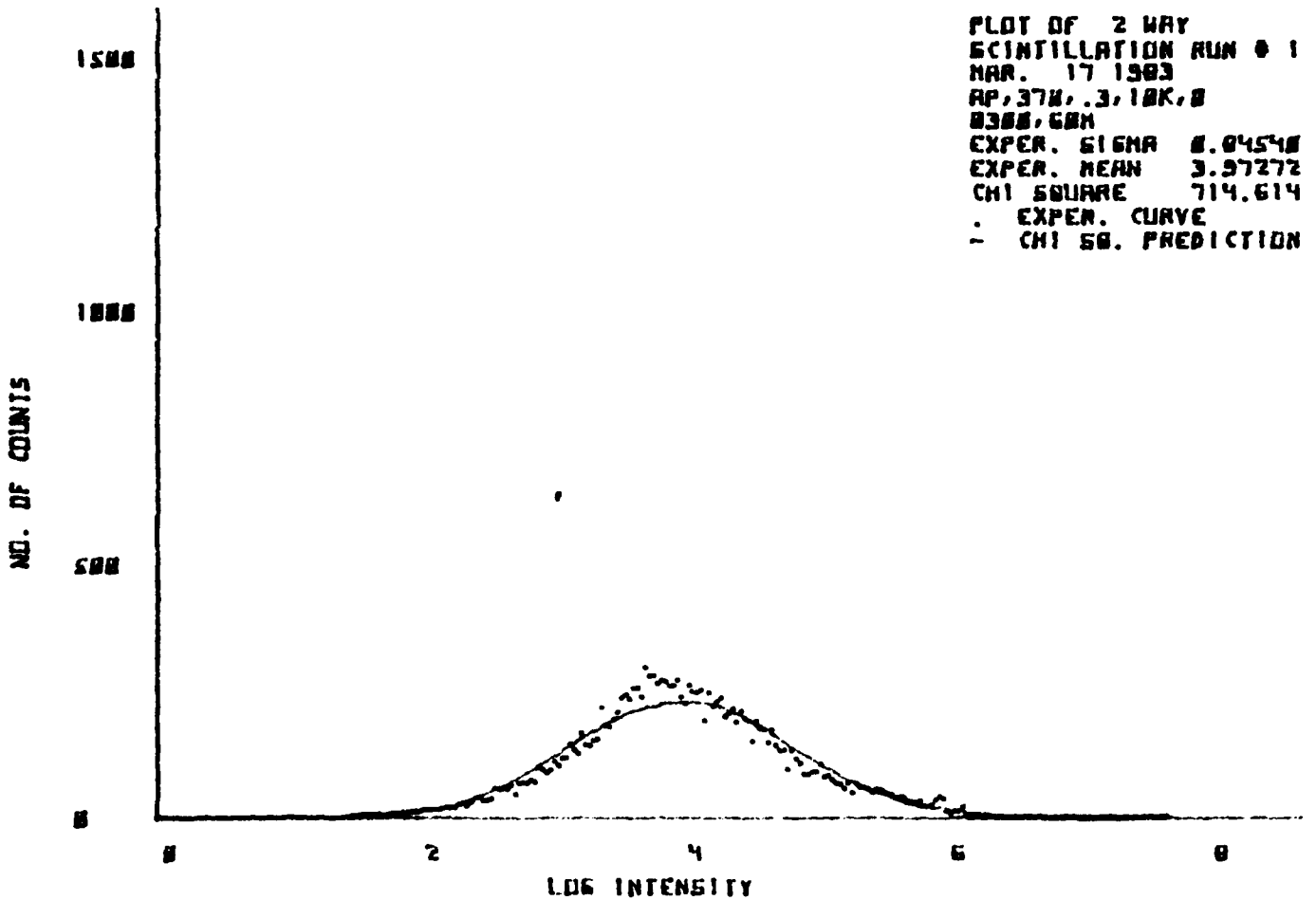

Figure 33. Scintillation Data and Theoretical Curve

DIRECT PATH SCINTILLATION DATA - 27 MARCH 1983

Disturbance Distance (Meters)	$\langle \sigma_i \rangle$
Quiet	.0498 ± .0027
1.0	.0755 ± .0012
5.8	.1076 ± .0084
10.7	.1538 ± .0068
15.5	.2308 ± .0160
20.4	.2694 ± .0215
25.3	.3221 ± .0110
30.1	.3347 ± .0220
35.0	.3550 ± .0210
39.8	.3783 ± .0345
44.7	.3989 ± .0110
49.5	.4165 ± .0046
54.4	.4191 ± .0111
60.0	.4404 ± .0326

FOLDED PATH SCINTILLATION DATA - 27 MARCH 1983

Disturbance Distance (Meters)	$\langle\sigma_i\rangle$	$(\langle\sigma_i\rangle^2 - \langle\sigma\rangle^2_{quiet}) \times 10^{-1}$	$C_T^2 (K^2/m^{-2/3})$	$(\langle\sigma_i\rangle^2 - \langle\sigma\rangle^2_{quiet}) \times 10^{-1}$ Normalized for C_T^2
Quiet	.07128 ± .00621			
1.0	.11025 ± .00185	.0708 ± .0097	195.58 ± 5.83	.0887 ± .0099
5.8	.18120 ± .01393	.2775 ± .0512	226.40 ± 5.08	.3003 ± .0540
10.7	.27058 ± .00755	.6813 ± .0418	191.98 ± 1.28	.8691 ± .0471
15.5	.40618 ± .02240	1.5990 ± .1821	191.65 ± 5.50	2.0451 ± .2331
20.4	.46893 ± .03068	2.1481 ± .2879	174.90 ± 1.40	3.0095 ± .3926
25.3	.55730 ± .02389	3.0550 ± .2664	215.00 ± 6.49	3.4827 ± .3971
30.1	.59370 ± .03751	3.4740 ± .4455	245.03 ± 5.67	3.4734 ± .6887
35.0	.62203 ± .02549	3.8184 ± .3173	209.43 ± 5.86	4.4713 ± .5044
39.8	.67425 ± .05509	4.4953 ± .7429	208.75 ± 2.90	5.2775 ± 1.2428
44.7	.69793 ± .02038	4.8202 ± .2847	209.85 ± 2.84	5.6300 ± .4871
49.5	.74173 ± .00555	5.4508 ± .0828	213.10 ± 1.65	6.2684 ± .1476
54.4	.76523 ± .01198	5.8049 ± .1835	194.47 ± 6.08	7.3142 ± .3344
60.0	.78405 ± .05385	6.0965 ± .8445	161.45 ± 2.41	9.2546 ± 1.5659

MAR. 27 1983
AP,370,.3,10K,0
1702, 10.7M
wavelengtn= 6.33E-07 meters

Scintillation measurements of Sigma
16384 samples for each measurement
Fixed range= 61 meters

# pts	Sigma	Chi Square
1:16384	0.1014	4.45E 02**
1:16384	0.2817	7.47E 02**
2:16385	0.1437	5.31E 02**
2:16383	0.2004	4.72E 02**
3:16385	0.1582	6.09E 02**
3:16383	0.2659	7.56E 02**
4:16385	0.1516	3.17E 02**
4:16383	0.2703	5.20E 02**

Figure 34. Scintillation Statistics

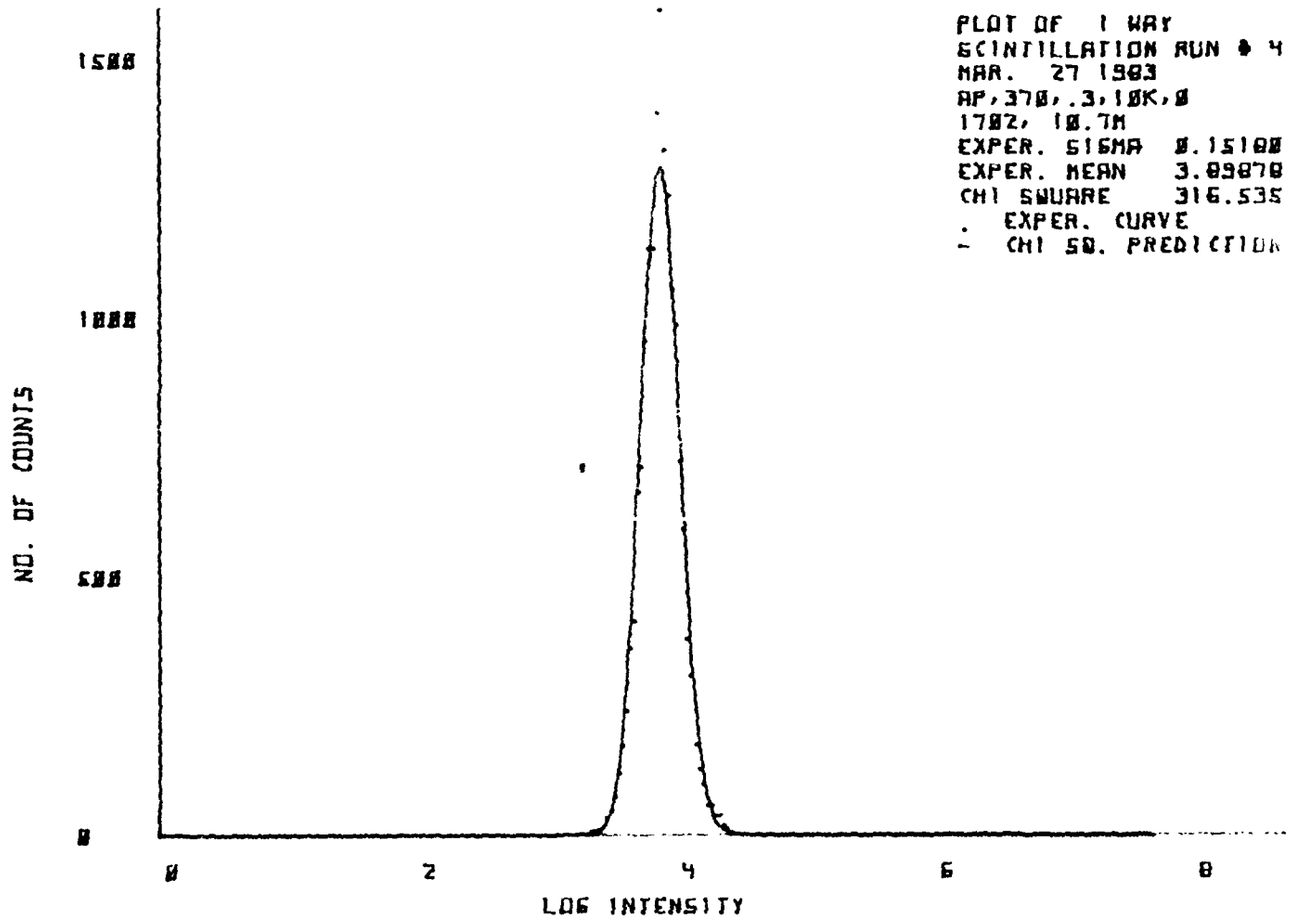

Figure 35. Scintillation Data and Theoretical Curve

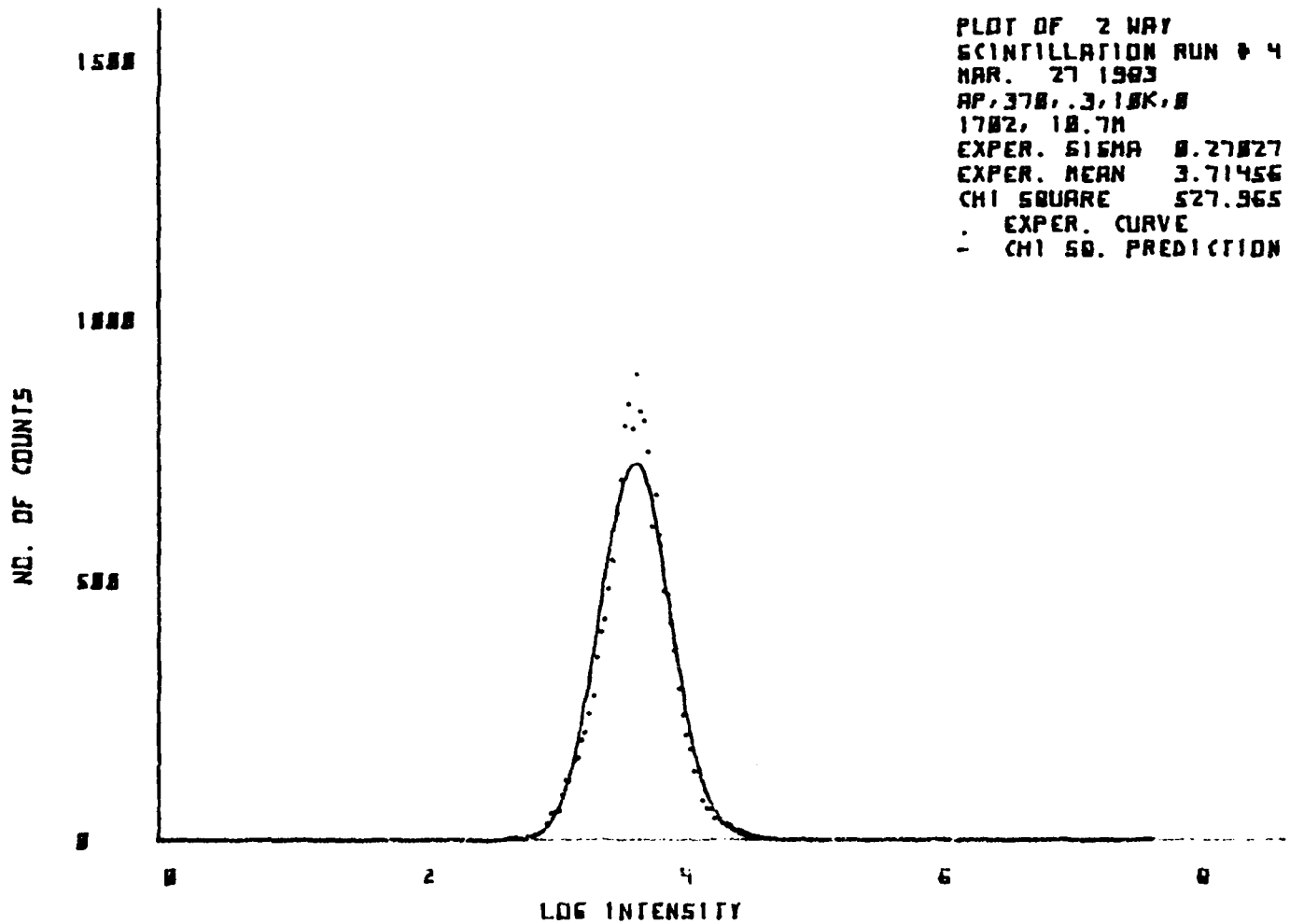

Figure 36. Scintillation Data and Theoretical Curve

MAR. 27 1983
AP,370,.3,10K,0
1919,30.1M
Wavelength= 6.33E-07 meters

Scintillation measurements of Sigma
16384 samples for each measurement
Fixed range= 61 meters

# pts	Sigma	Chi Square
1:16384	0.3494	3.45E 02**
1:16381	0.6149	4.58E 02**
2:16378	0.3402	7.55E 02**
2:16366	0.5916	4.05E 02**
3:16383	0.2973	3.27E 02**
3:16383	0.5341	3.95E 02**
4:16385	0.3517	3.33E 02**
4:16383	0.6340	4.60E 02**

Figure 37. Scintillation Statistics

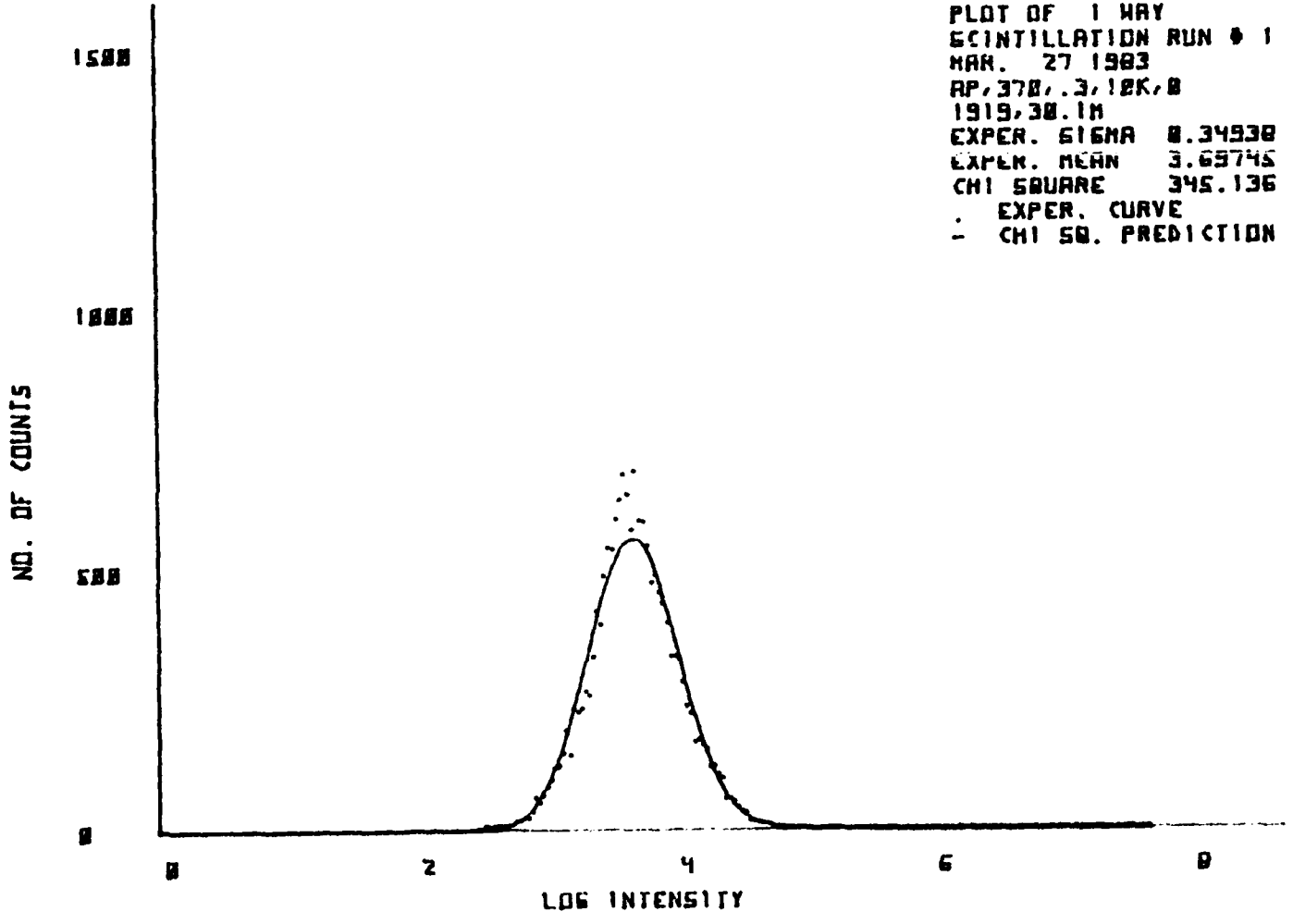

Figure 38. Scintillation Data and Theoretical Curve

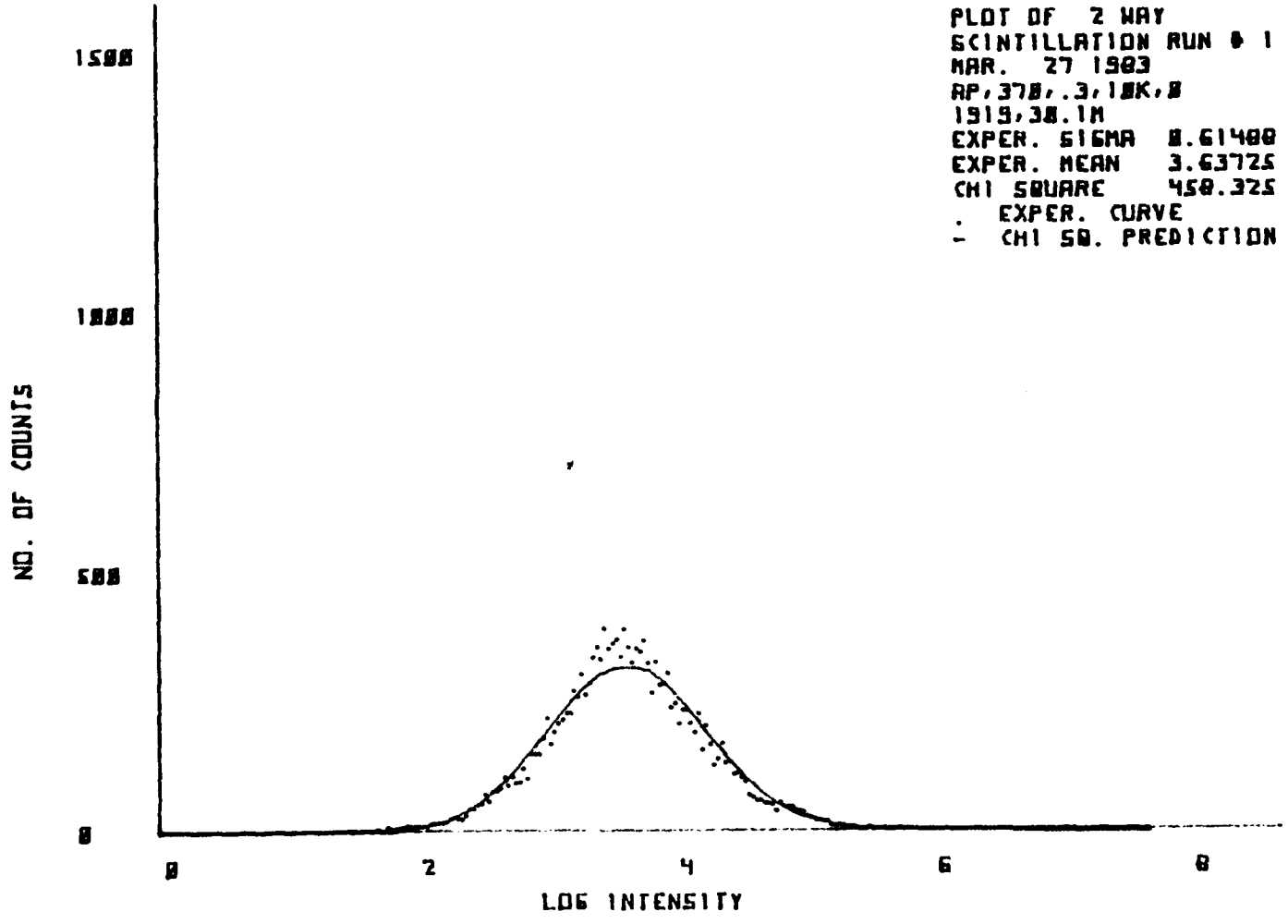

Figure 39. Scintillation Data and Theoretical Curve

DIRECT PATH SCINTILLATION DATA - 30 MARCH 1983

Disturbance Distance (Meters)	$\langle\sigma_i\rangle$	$(\langle\sigma_i\rangle^2 \langle\sigma\rangle_{quiet}^2) \times 10^{-2}$	$C_T^2 (K^2/m^{-2/3})$	$(\langle\sigma_i\rangle^2 \langle\sigma\rangle_{quiet}^2 \times 10^{-2}$ Normalized for C_T^2
Quiet	.0595 ± .0004		.2017 ± .021	
1.0	.0667 ± .0003	.0905 ± .0062	125.33 ± 4.24	.1165 ± .0062
5.8	.0759 ± .0012	.2216 ± .0188	83.67 ± 6.41	.4272 ± .0189
10.7	.1058 ± .0013	.7662 ± .0279	132.05 ± 9.21	.9363 ± .0284
15.5	.1043 ± .0007	.7341 ± .0198	142.47 ± 11.03	.8310 ± .0201
20.4	.1231 ± .0067	1.1604 ± .1650	144.35 ± 5.71	1.2973 ± .1687
25.3	.1504 ± .0040	1.9090 ± .1204	141.63 ± 11.73	1.3217 ± .1250
30.1	.1727 ± .0048	2.6297 ± .1659	154.05 ± 6.48	2.7533 ± .1744
35.0	.1465 ± .0028	1.7925 ± .0822	161.33 ± 9.32	1.7925 ± .0851
39.8	.1658 ± .0071	2.3961 ± .2355	156.85 ± 4.14	2.4655 ± .2466
44.7	.1496 ± .0065	1.8843 ± .1945	145.28 ± 9.23	2.0916 ± .2017
49.5	.1400 ± .0035	1.6056 ± .0981	147.18 ± 6.55	1.7597 ± .1012
54.4	.1004 ± .0019	.6558 ± .0385	143.43 ± 3.17	.7378 ± .0390
60.0	.0751 ± .0008	.2099 ± .0129	133.48 ± 3.20	.2538 ± .0129

FOLDED PATH SCINTILLATION DATA - 30 MARCH 1983

Disturbance Distance (Meters)	$\langle\sigma_i\rangle$		$(\langle\sigma_i\rangle^2 \langle\sigma\rangle^2_{quiet}) \times 10^{-1}$		$C_T^2 (K^2/m^{-2/3})$		$(\langle\sigma_i\rangle^2 \langle\sigma_{quiet}\rangle^2) \times 10^{-1}$ Normalized for C_T^2	
Quiet	.1129	± .0005			.2017	± .021		
1.0	.1324	± .0044	.0476	± .0017	125.33	± 4.24	.0613	± .0181
5.8	.1364	± .0047	.0585	± .0129	83.67	± 6.41	.1127	± .0130
10.7	.1396	± .0025	.0674	± .0071	132.05	± 9.21	.0823	± .0072
15.5	.1496	± .0040	.0964	± .0120	142.47	± 11.03	.1091	± .0123
20.4	.1887	± .0116	.2286	± .1061	144.35	± 5.71	.2555	± .0543
25.3	.2998	± .0171	.7711	± .1025	141.63	± 11.73	.8783	± .1173
30.1	.4574	± .0066	1.9642	± .0603	154.05	± 6.48	2.0565	± .0806
35.0	.4490	± .0064	1.8883	± .0586	161.33	± 9.32	1.9642	± .0767
39.8	.4459	± .0110	1.8605	± .0981	156.85	± 4.14	1.9144	± .1296
44.7	.4089	± .0225	1.4795	± .1804	145.28	± 9.23	1.6422	± .2276
49.5	.5154	± .0037	2.5291	± .0382	147.18	± 6.55	2.7719	± .0541
54.4	.5513	± .0079	2.9118	± .0871	143.43	± 3.17	3.2758	± .1282
60.0	.6678	± .0044	4.3314	± .0588	133.48	± 3.20	5.2351	± .0972

```
MAR.  30 1983
AF,370,100,100K,0
1641, 5.8M
wavelength=    0.33E-07 meters


Scintillation measurements of Sigma
16384 samples for each measurement
Fixed range=     61 meters

    # pts        Sigma     Chi Square

  1:16385      0.0773     6.30E 02**
  1:16383      0.1507     5.63E 02**
  2:16385      0.0760     3.81E 02**
  2:16383      0.1336     3.72E 02**
  3:16385      0.0763     2.95E 02**
  3:16383      0.1367     2.23E 02
  4:16385      0.0716     3.71E 02**
  4:16383      0.1245     3.52E 02**
```

Figure 40. Scintillation Statistics

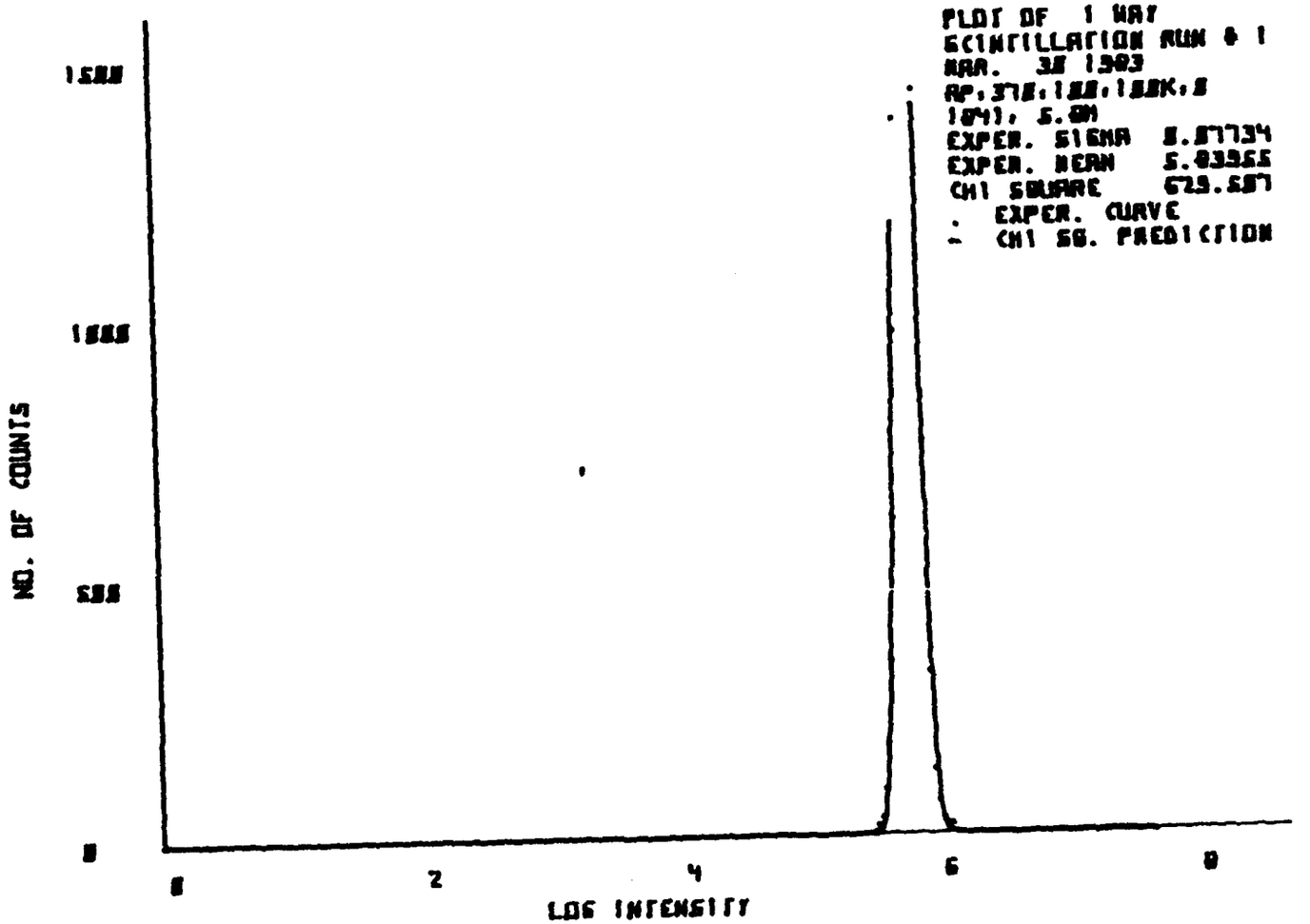

Figure 41. Scintillation Data and Theoretical Curve

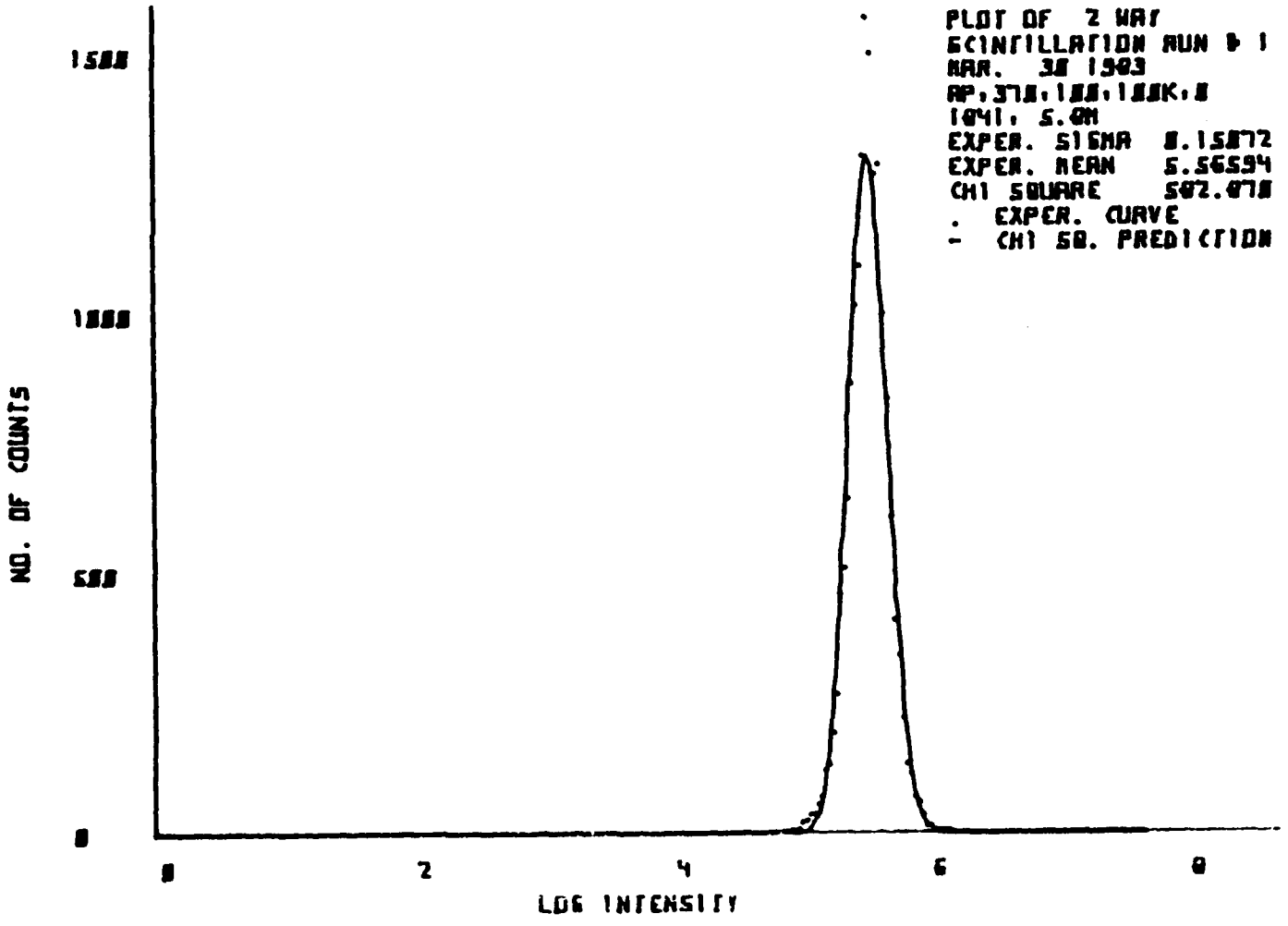

Figure 42. Scintillation Data and Theoretical Curve

MAR. 30 1983
AP,370,100,100K,0
1535, 49.5M
wavelength= 6.33E-07 meters

Scintillation measurements or Sigma
16384 samples for each measurement
Fixed range= 61 meters

# pts	Sigma	Chi Square
1:16385	0.1313	5.12E 02**
1:16383	0.5223	2.27E 03**
2:16385	0.1403	9.14E 02**
2:16383	0.5043	2.00E 03**
3:16385	0.1375	7.70E 02**
3:16383	0.5130	1.78E 03**
4:16385	0.1506	1.29E 03**
4:16383	0.5221	1.40E 03**

Figure 43. Scintillation Statistics

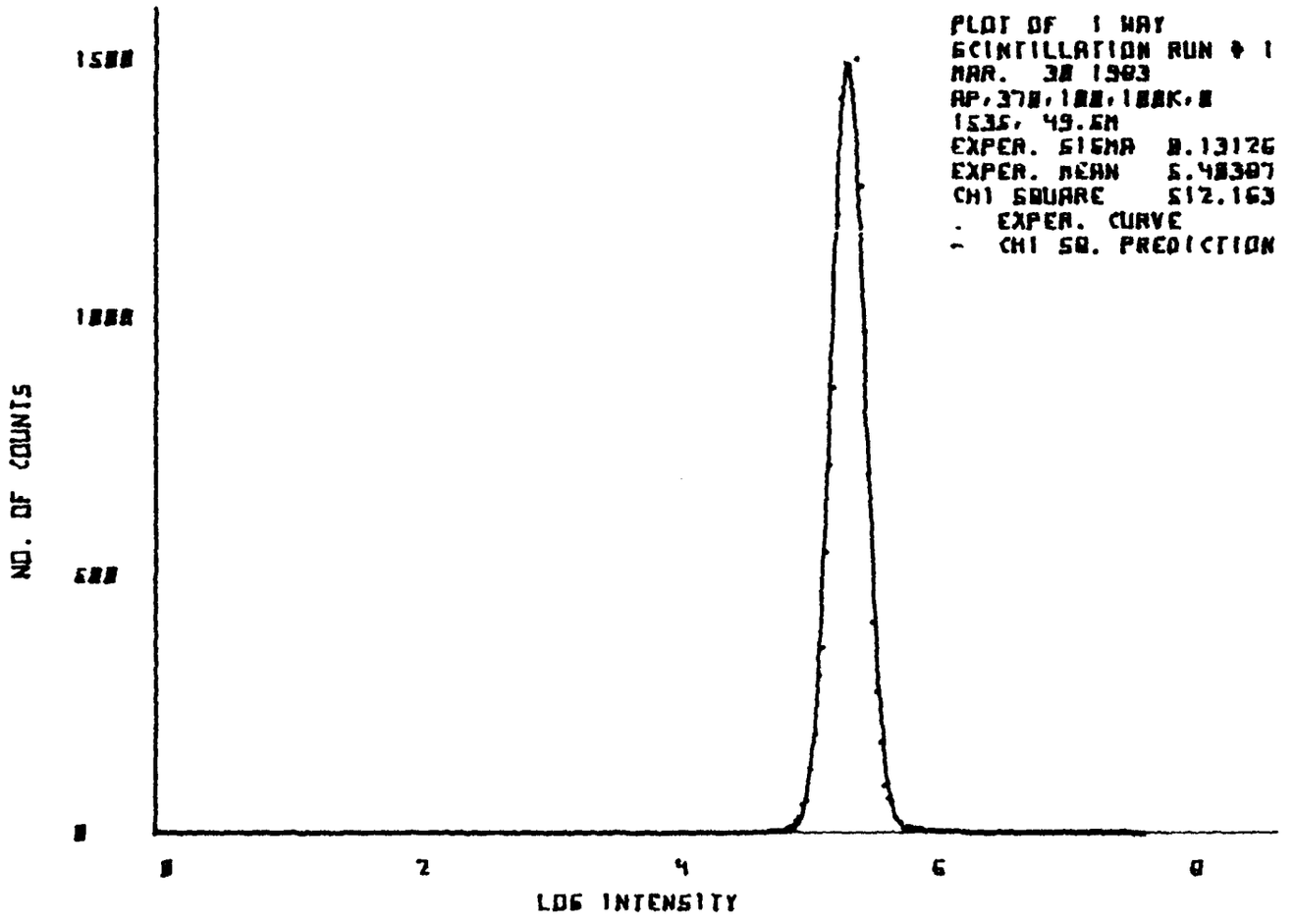

Figure 44. Scintillation Data and Theoretical Curve

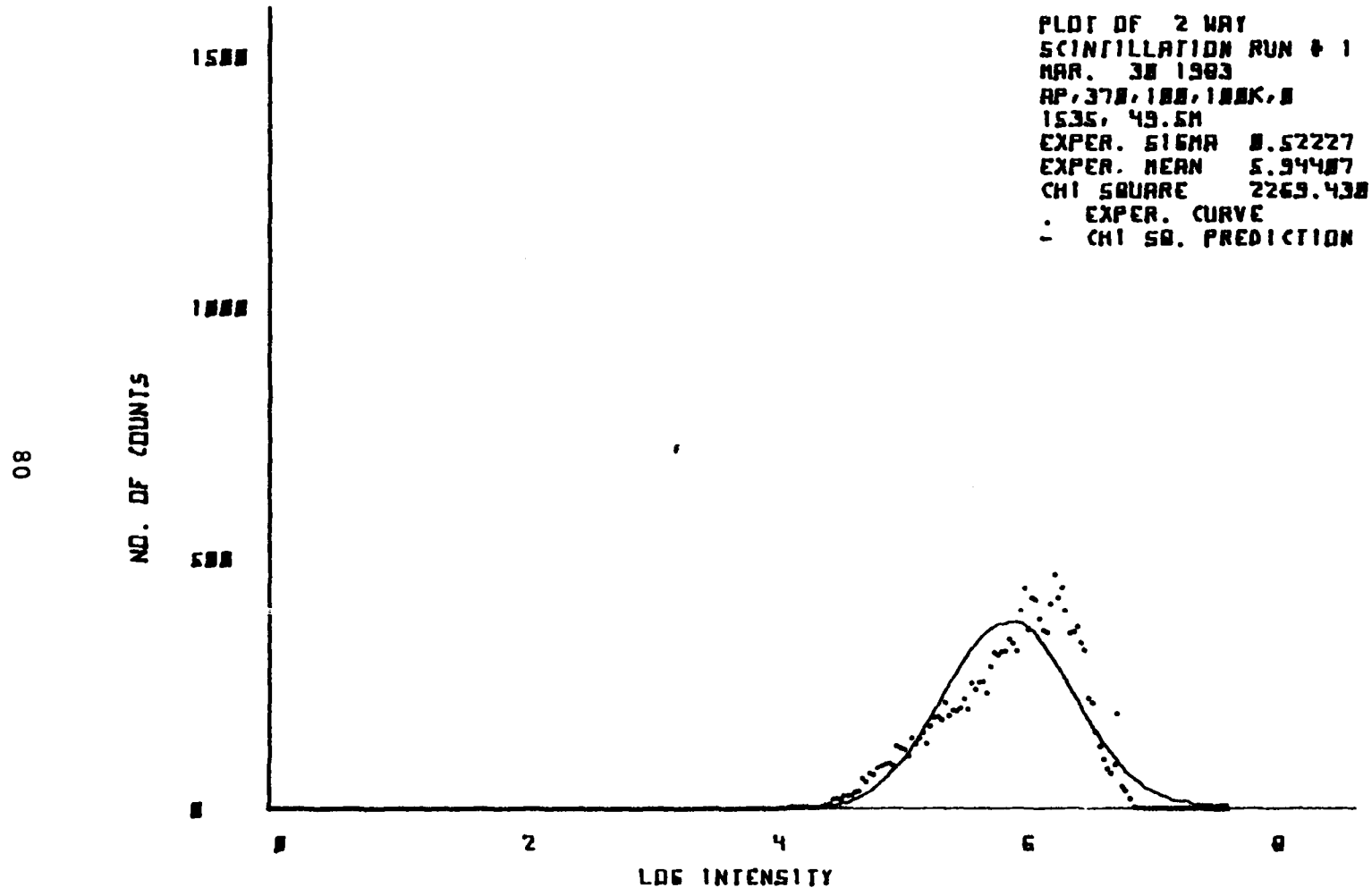

Figure 45. Scintillation Data and Theoretical Curve

DIRECT PATH SCINTILLATION DATA - 13 APRIL 1983

Disturbance Distance (Meters)	$\langle\sigma_i\rangle$			$(\langle\sigma_i\rangle^2 - \langle\sigma\rangle^2_{quiet}) \times 10^{-2}$			$C_T (K^2/m^{-2/3})$			$(\langle\sigma_i\rangle^2 - \langle\sigma_{quiet}\rangle^2) \times 10^{-2}$ Normalized for C_T^2		
Quiet	.0591	±	.0016				.3345	±	.04			
1.0	.0594	±	.0011	.0032	±	.0600	140.88	±	4.72	.0034	±	.0612
5.8	.0788	±	.0011	.2723	±	.0622	110.50	±	2.10	.3688	±	.0626
10.7	.0984	±	.0019	.6193	±	.0705	126.15	±	3.00	.7347	±	.0714
15.5	.1277	±	.0042	1.2824	±	.1192	96.90	±	4.43	1.9805	±	.1222
20.4	.1404	±	.0186	1.6222	±	.5257	82.35	±	1.15	2.9476	±	.5425
25.3	.1364	±	.0054	1.5101	±	.1590	86.60	±	2.85	2.6095	±	.1637
30.1	.1076	±	.0071	.8008	±	.1641	90.18	±	1.42	1.3422	±	.3377
35.0	.1307	±	.0030	1.3586	±	.0986	90.59	±	5.40	2.2443	±	.1013
39.8	.1409	±	.0091	1.6349	±	.2633	102.65	±	7.00	2.3835	±	.2718
44.7	.1315	±	.0083	1.3789	±	.2263	112.84	±	4.47	1.8287	±	.2325
49.5	.1391	±	.0039	1.5852	±	.1239	149.65	±	3.70	1.5852	±	.1277
54.4	.1291	±	.0036	1.3164	±	.1105	144.25	±	8.01	1.3657	±	.1134
60.0	.0834	±	.0018	.3466	±	.0669	138.55	±	2.38	.3744	±	.0714

FOLDED PATH SCINTILLATION DATA - 13 APRIL 1983

Disturbance Distance (Meters)	$\langle\sigma_i\rangle$	$(\langle\sigma_i\rangle^2 - \langle\sigma\rangle^2_{quiet})\,10^{-1}$	$C_T^2\,(K^2/m^{-2/3})$	$(\langle\sigma_i\rangle^2 - \langle\sigma\rangle^2_{quiet})\times 10^{-1}$ Normalized for C_T^2
Quiet	.0680 ± .0017		.3345 ± .021	
1.0	.1180 ± .0008	.0931 ± .0030	140.88 ± 4.72	.0989 ± .0030
5.8	.1344 ± .0018	.1344 ± .0054	110.50 ± 2.10	.1820 ± .0055
10.7	.1660 ± .0012	.2294 ± .0046	126.15 ± 3.00	.2721 ± .0048
15.5	.2268 ± .0046	.4681 ± .0210	96.90 ± 4.43	.7229 ± .0229
20.4	.2050 ± .0094	.3741 ± .0386	82.35 ± 1.15	.6798 ± .0610
25.3	.2502 ± .0058	.5797 ± .0291	86.60 ± 2.85	1.0018 ± .0323
30.1	.2385 ± .0092	.5227 ± .0278	90.18 ± 1.42	.8764 ± .0305
35.0	.2183 ± .0056	.4305 ± .0246	90.59 ± 5.40	.7112 ± .0266
39.8	.3085 ± .0101	.9054 ± .0624	102.65 ± 7.00	1.3200 ± .0728
44.7	.3709 ± .0075	1.3293 ± .0557	112.84 ± 4.47	1.7629 ± .0689
49.5	.4476 ± .0130	1.9573 ± .1164	149.65 ± 3.70	1.9573 ± .1554
54.4	.51905 ± .0155	2.6479 ± .1609	144.25 ± 8.01	2.7470 ± .1909
60.0	.6745 ± .0136	4.5033 ± .1635	138.55 ± 2.38	4.8641 ± .3071

APR. 13 1983
AP,370,100,10K,0
2141, 15.5K
wavelength= 0.33E-07 meters

Scintillation measurements of Sigma
16384 samples for each measurement
fixed range= 61 meters

# pts	Sigma	Chi Square
1:16385	0.1223	1.45E 03**
1:16383	0.2117	1.21E 03**
2:16385	0.1160	1.30E 03**
2:16383	0.2274	8.11E 02**
3:16385	0.1405	2.15E 03**
3:16383	0.2321	1.30E 03**
4:16385	0.1293	1.77E 03**
4:16383	0.2389	9.67E 02**

Figure 46. Scintillation Statistics

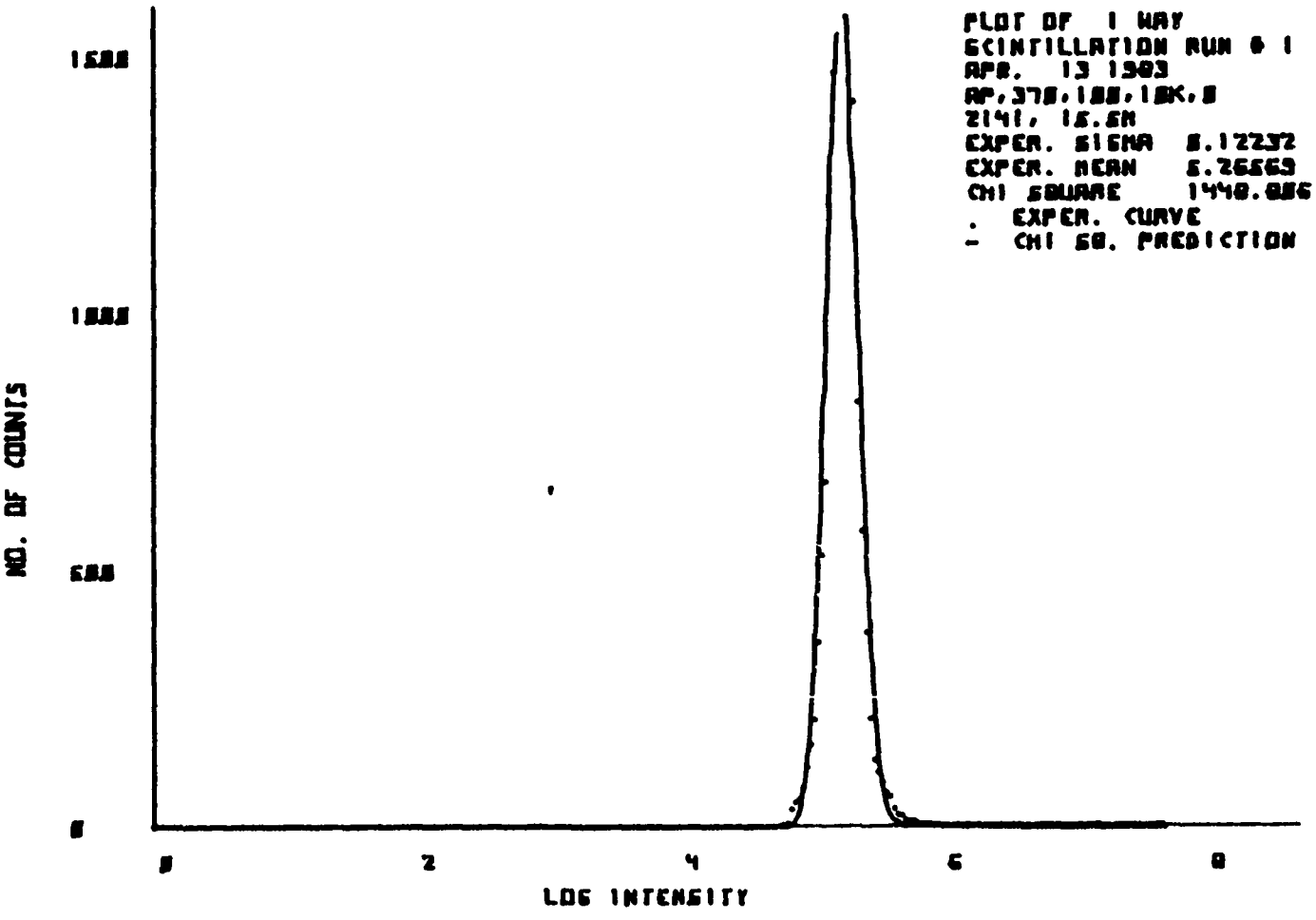

Figure 47. Scintillation Data and Theoretical Curve

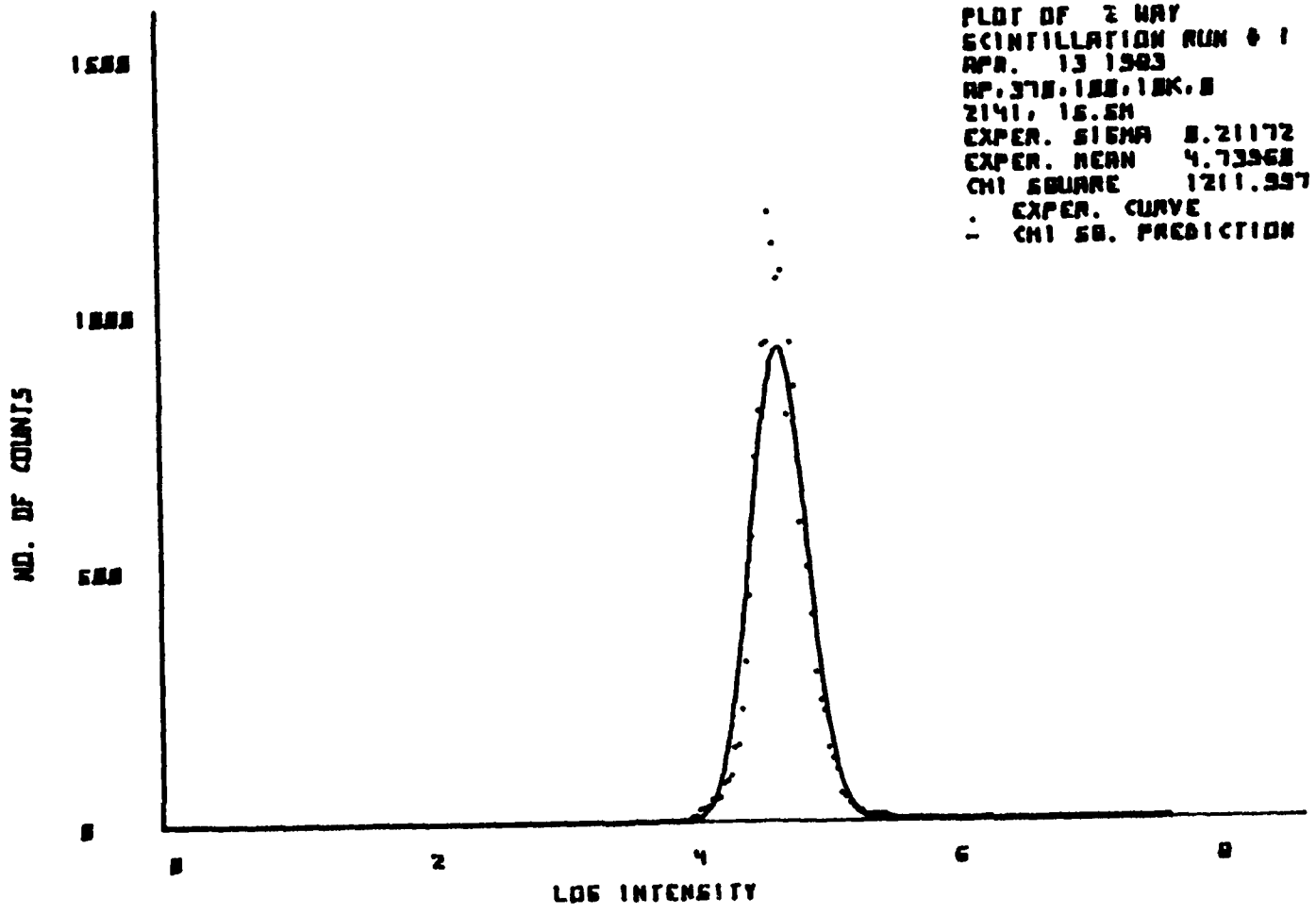

Figure 48. Scintillation Data and Theoretical Curve

APR. 13 1983
AP,370,100,10K,0
1800, 54.4M
Wavelength= 6.33E-07 meters

Scintillation measurements of Sigma
16364 samples for each measurement
Fixed range= 61 meters

# pts	Sigma	Chi Square
1:16379	0.1276	1.52E 03**
1:16359	0.5721	6.19E 02**
2:16385	0.1223	1.33E 03**
2:16363	0.4963	6.13E 02**
3:16385	0.1252	1.35E 03**
3:16363	0.4998	9.06E 02**
4:16374	0.1409	1.47E 03**
4:16347	0.5080	1.38E 03**

Figure 49. Scintillation Statistics

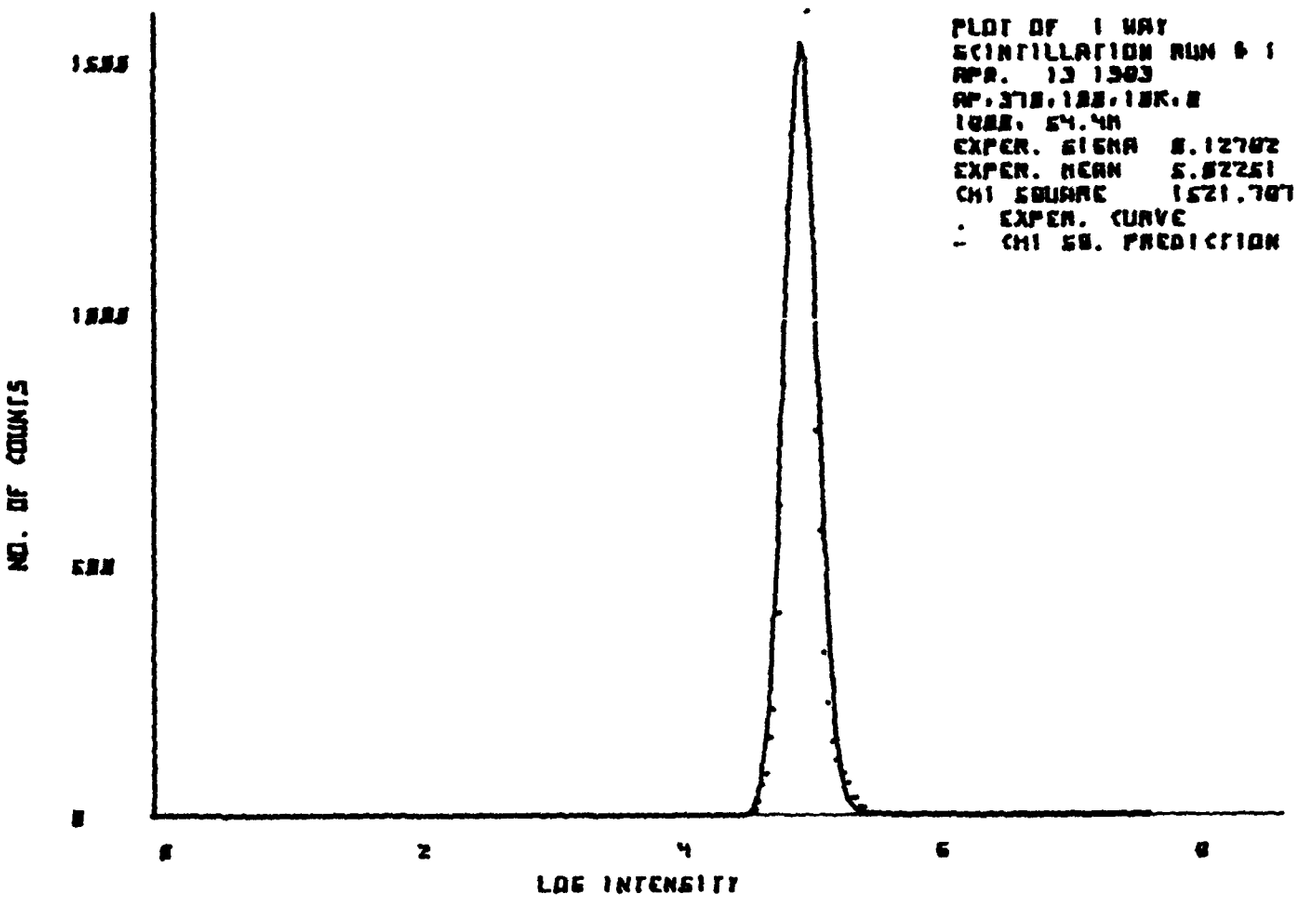

Figure 50. Scintillation Data and Theoretical Curve

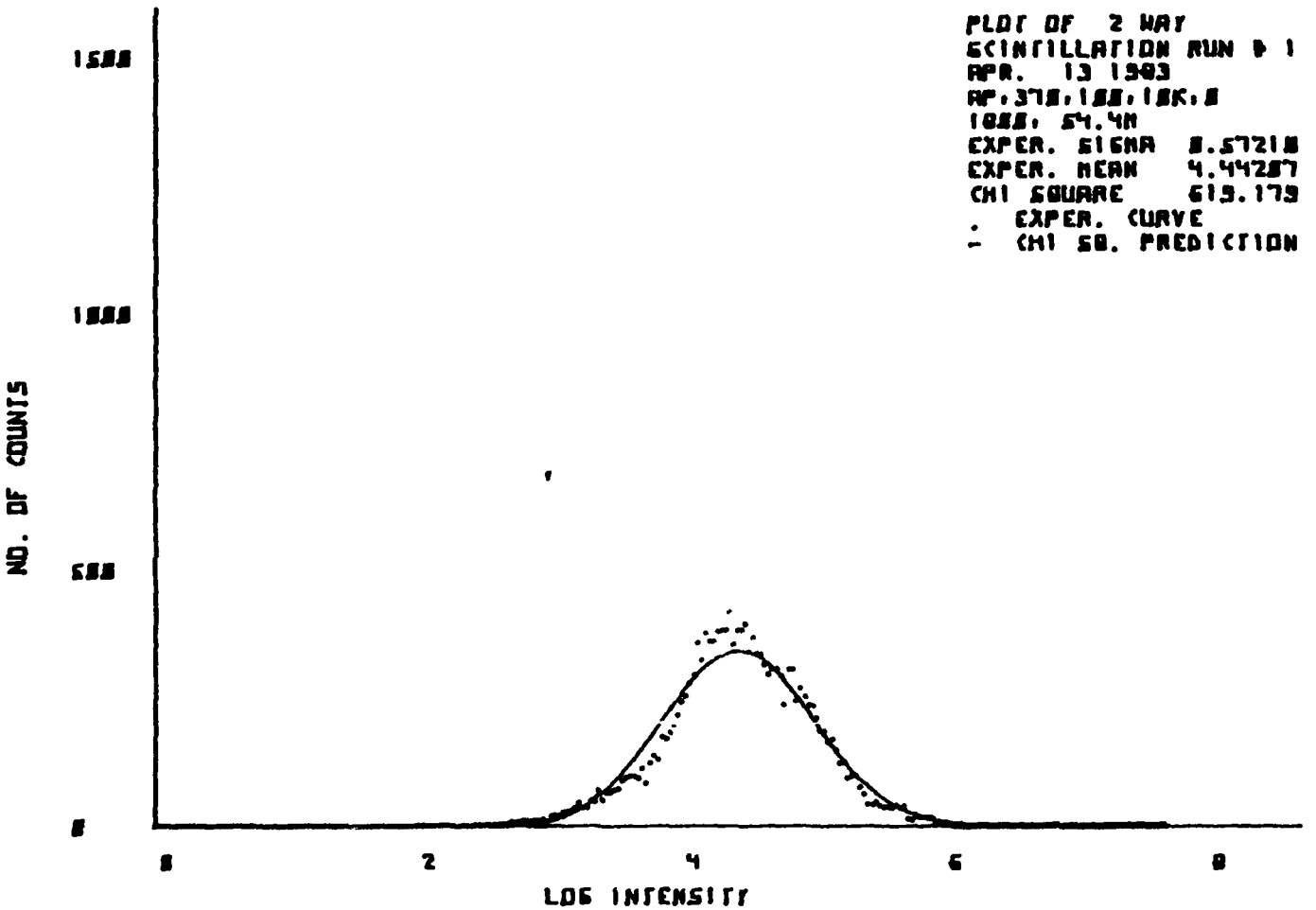

Figure 51. Scintillation Data and Theoretical Curve

APR, 13 1983
AP,370,100,10R,0
1732, 60M
wavelength= 6.33E-07 meters

Scintillation measurements of Sigma
16384 samples for each measurement
Fixed range= 61 meters

# pts	Sigma	Chi Square
1:16384	0.0794	3.69E 02**
1:16382	0.6340	2.37E 03**
2:16382	0.0814	2.72E 02
2:16382	0.6923	1.96E 03**
3:16384	0.0886	7.29E 02**
3:16377	0.6657	1.52E 03**
4:16382	0.0840	1.00E 02
4:16374	0.7054	2.51E 03**

Figure 52. Scintillation Statistics

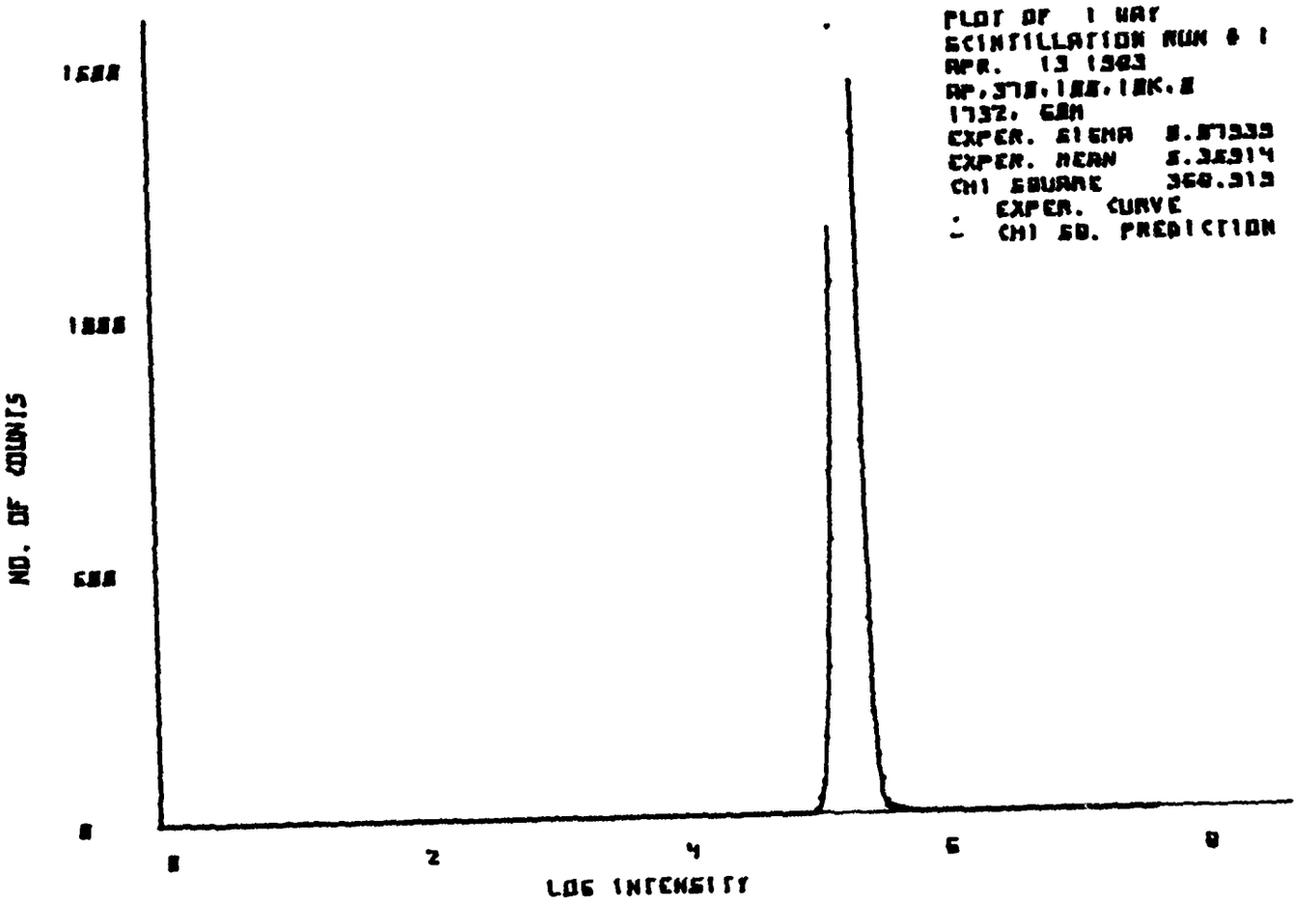

Figure 53. Scintillation Data and Theoretical Curve

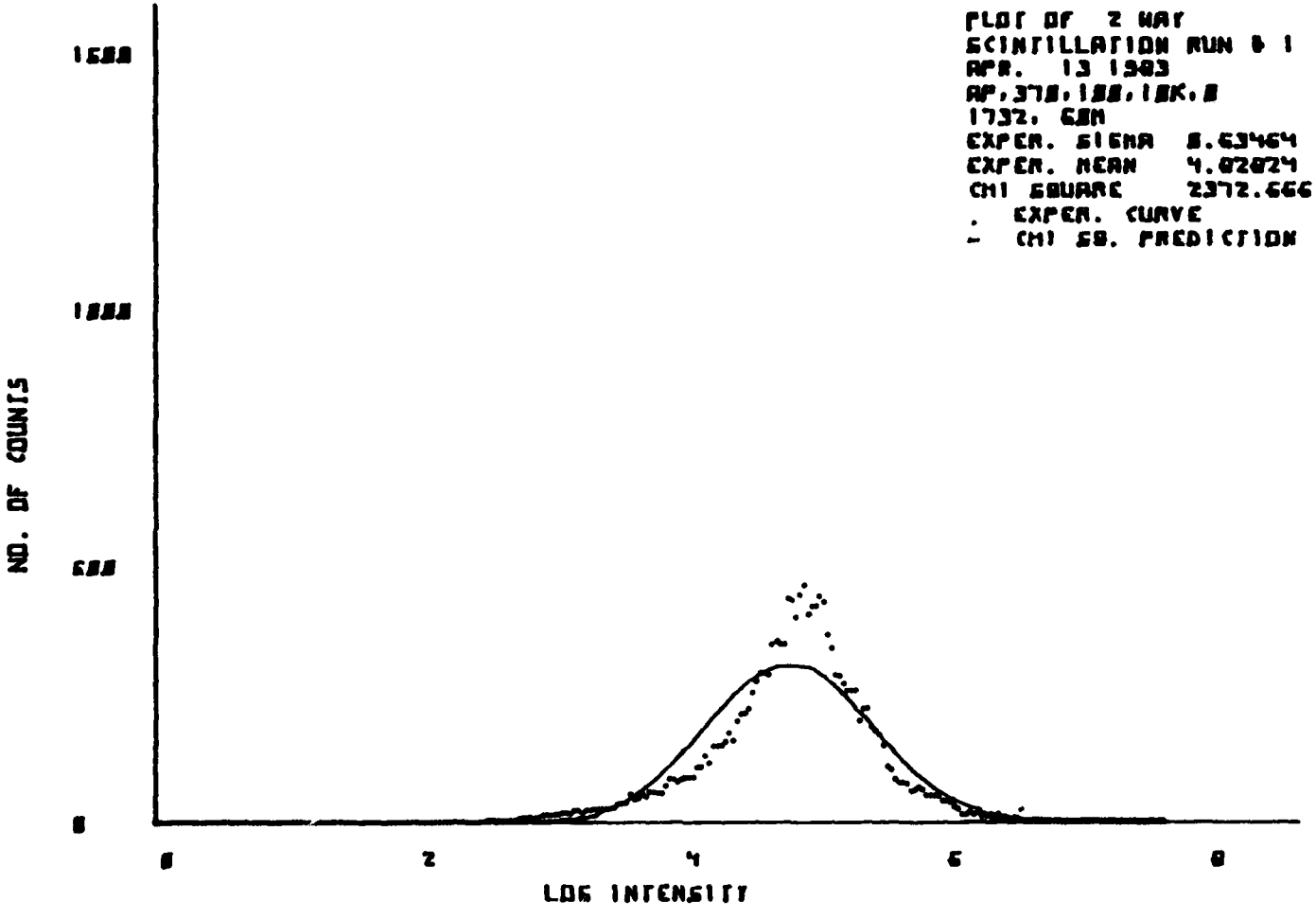

Figure 54. Scintillation Data and Theoretical Curve

LIST OF REFERENCES

1. Tatarski, V. I., The Effects of the Turbulent Atmosphere on Wave Propagation, Keter Press Binding, Israel, 1971.

2. Strohbehn, J. W., gen. ed., Topics in Applied Physics, v. 25, Springer-Verlag, 1978, "The Classical Theory of Wave Propagation in a Turbulent Medium", by S. F. Clifford.

3. Fried, D. L., "Propagation of a Spherical Wave in a Turbulent Medium", JOSA, v. 57, p. 175, 1967.

4. Clifford, S. F., Ochs, G. R., Lawrence, R. S., "Saturation of Optical Scintillation by Strong Turbulence", JOSA v. 64, p. 148, 1974.

5. Lutomirski, R. F., and Yura, H. T., "Propagation of a Finite Optical Beam in an Inhomogeneous Medium", Appl. Opt., v. 10, p. 1652, 1971.

6. Fante, R. L., "Electromagnetic Beam Propagation in Turbulent Media; An Update", IEEE Proc., v. 68, p. 1424, 1980.

7. Ze'evi, Avihu, Optical Scintillation Along Folded Paths, PhD. Thesis, Naval Postgraduate School, Monterey, March 1982.

8. Naval Postgraduate School Report 61-78-003, Optical Resolution in the Turbulent Atmosphere of the Marine Boundary Layer, By E. C. Crittenden, A. W. Cooper, E. A. Milne, G. W. Rodeback, R. L. Armstead, S. H. Kalmback, D. Land, B. Katz, February 1978.

9. Hodgini, Thomas J., Optical Scintillation Measurements for Single and Folded Paths, Master's Thesis, Naval Postgraduate School, March 1982.

10. Speer, Bradford A., and Parker, Frederick H., Measurements of Direct Path and Folded Path Optical Scintillation, Master's Thesis, Naval Postgraduate School, December 1982.

11. Flenniken, Robert J., Weighting for the Modulation Transfer Function, Master's Thesis, Naval Postgraduate April 1983.

INITIAL DISTRIBUTION LIST

		No. Copies
1.	Defense Technical Information Center Cameron Station Alexandria, Virginia 22314	2
2.	Library, Code 0142 Naval Postgraduate School Monterey, California 93940	2
3.	G. E. Schacher, Chairman, Code 61Sq Department of Physics Naval Postgraduate School Monterey, California 93940	2
4.	E. C. Crittenden, Jr., Code 61Ct Department of Physics Naval Postgraduate School Monterey, California 93940	2
5.	Professor E. A. Milne, Code 61Mn Department of Physics Naval Postgraduate School Monterey, California 93940	4
6.	M. C. Drong, Code 1230 Pacific Missile Test Center Point Mugu, NAS, California 93042	1
7.	A. G. Costantine Department of Physics USMA West Point, NY 10996	2
8.	R. J. Flenniken So. 1017 Wright Blvd Liberty Lake, Washington 99019	1
10.	Captain David Anhalt, Code 1230.2 Pacific Missile Range Point Mugu, NAS, California 93042	1


DAT
FILM